

A kinematic study and membership analysis of the Lupus star-forming region[★]

P.A.B. Galli¹, C. Bertout², R. Teixeira¹, and C. Ducourant³

¹ Instituto de Astronomia, Geofísica e Ciências Atmosféricas, Universidade de São Paulo, Rua do Matão, 1226 - Cidade Universitária, 05508-900, São Paulo - SP, Brazil

e-mail: galli@astro.iag.usp.br

² Institut d'Astrophysique, 98bis, Bd. Arago, 75014 Paris, France

³ Observatoire Aquitain des Sciences de l'Univers, CNRS-UMR 5804, BP 89, Floirac, France

Received / Accepted

ABSTRACT

Aims. A precise determination of the distance to individual stars is required to reliably determine the fundamental parameters (mass and age) of young stellar objects. This paper is dedicated to investigating the kinematic properties of the Lupus moving group of young stars with the primary objective of deriving individual parallaxes for each group member.

Methods. We identify those stars in the Lupus star-forming region that define the comoving association of young stars by utilizing our new and improved convergent point search method that allows us to derive the precise position of the convergent point of the comoving association from the stars' proper motions. We used published proper motion catalogs and searched the literature for radial velocities, which are needed to compute individual parallaxes. We supplemented the radial velocity data with new measurements from spectroscopic observations performed with the FEROS spectrograph mounted on the MPG/ESO 2.2m telescope at La Silla.

Results. We identify a comoving group with 109 pre-main sequence stars and candidates that define the kinematic properties of the Lupus low-mass star-forming region. We derive individual parallaxes for stars with known radial velocity and tentative parallaxes for the remaining group members by assuming that all stars share the same space motion. The convergent point method, combined with the k-NN algorithm, makes it possible to distinguish the Lupus and Upper Centaurus Lupus stars from the adjacent Scorpius-Centaurus association. We find significant depth effects in this region and show that the classical T Tauri stars, located in the close vicinity of the Lupus molecular clouds, form a background population, while the weak-emission line T Tauri stars are dispersed not only in angular extent but also in depth.

Conclusions. The newly derived individual parallaxes will be used in a forthcoming paper to refine the masses and ages of Lupus T Tauri stars, with the aim of better constraining the lifetimes of their circumstellar, protoplanetary disks.

Key words. methods: data analysis - technique: radial velocities - astrometry - parallaxes - proper motions - stars: distances - stars: kinematics and dynamics - open clusters and associations: individual: Lupus

1. Introduction

The inferred fundamental parameters of T Tauri stars (TTSs), the young solar-type pre-main sequence stars first discovered by Joy (1945), are sensitive to their assumed distance. TTSs are usually associated with molecular clouds, the distances of which can be estimated, say, from the photometry of a few bright stars enshrouded in reflection nebulosity (see, for example, Racine 1968) or from 2MASS extinction maps combined with known stellar parallaxes (Lombardi et al. 2008). The distances to the nearby star-forming regions (SFRs) are thus known to relatively good accuracy, providing a first estimate of the distances to the members of the stellar population associated with them. Although these average parallaxes provide valuable information, we must know the distances to the individual members of the young associations more precisely to better constrain their ages and masses by comparing observed stellar properties to evolutionary models.

TTSs are late-type objects and usually faint in the visible, suffering typically from 1 to 2 magnitudes of extinction in that

range, while the nearby SFRs to which they belong are typically in the distance range 0.1 – 1 kpc. Parallax determination from the ground is usually impossible for these objects, and they even presented a challenge for the HIPPARCOS mission (ESA 1997), which observed only a few of them. Bertout et al. (1999) computed new astrometric solutions using the HIPPARCOS data for groups of TTSs in various SFRs, thus providing post-HIPPARCOS average distances to these groups.

Some progress in determining the distance of individual TTSs has been made in recent years, using two different methods. Loinard and collaborators used the Very Long Baseline Array (VLBA) to determine parallaxes of a few selected objects, mainly in the Taurus-Auriga SFR (Loinard et al. 2007; Torres et al. 2007, 2009; Dzib et al. 2010, 2011; Torres et al. 2012). The VLBA data allow for a very precise parallax determination, but the method is observationally intensive, limiting its application to a few remarkable stars. Another approach rests on the fact that the members of young associations share the same spatial motion and uses their proper motions to determine individual parallaxes for members of some nearby associations. This was done, for example, for the TW Hydrae association by Mamajek (2005) and for the Taurus-Auriga SFR by Bertout & Genova (2006). The

[★] Based partly on observations collected at the European Southern Observatory, Chile (ESO Programme 087.C-0315).

derived parallaxes using this method are not as precise as those obtained by VLBA observations, but it yields usable parallaxes for all members of the moving group that have measured radial velocities.

Thus, while we have progressed, we are still far from knowing the distances to the large sample of pre-main sequence stars (PMSs), which is required to study such timely topics as the effect of differing protostellar environments on disk lifetimes and the timescales of planet formation. The situation will change considerably with the launch of the Gaia mission, because its instruments will measure the parallaxes and proper motions of millions of faint stars. Although the satellite's launch date is 2013, its catalog will be published several years later, so one would appreciate making some progress in determining the distances of TTSs in the meantime. Also, the astrometric methods that are developed and tested for this purpose will certainly be useful in the Gaia era.

In this paper, we study the largest southern SFR, located in Lupus, using the recently developed new version of the convergent point (CP) method presented by Galli et al. (2012). Section 2 is devoted to a brief presentation of the Lupus SFR and its previous distance determinations, while Sect. 3 discusses the sample of Lupus candidate stars found in recent catalogs and proper motion information needed for the CP analysis. Section 4 discusses our search for radial velocity data, including observations carried out for a number of stars in our sample with FEROS mounted on the 2.2m MPG/ESO telescope at La Silla, Chile. The CP and membership analysis are discussed in Sect. 5, while Sect. 6 presents the parallax computations for the moving group members. We discuss the results of this investigation in Sect. 7. Finally, our conclusions are given in Sect. 8.

2. The Lupus association of young stars

The Lupus dark cloud complex is a low-mass star-forming region that contains four main star-forming clouds (Lupus 1 to 4) and constitutes one of the richest nearby associations of TTSs. Many of the Lupus TTSs have been identified from ROSAT X-ray observations and from the spectroscopic surveys conducted by Krautter et al. (1997) and Wichmann et al. (1997a,b). These surveys showed that the Lupus molecular clouds are surrounded by an extended halo of late-type, X-ray active stars, which bear resemblance to the so-called weak emission-line TTSs (WTTs), the X-ray active TTSs without circumstellar accretion disks (Walter 1986). If the ROSAT-detected objects were all WTTs belonging to the Lupus association, then they would greatly exceed the number of so-called classical TTSs (CTTSs), the TTS subgroup showing evidence of circumstellar accretion disks (Bertout 1987; Bertout et al. 1988). Lupus CTTSs were identified by Schwartz (1977) on the basis of their association with the molecular clouds and their H α emission. This early census of Lupus young stars has recently been expanded by infrared observations with the *Spitzer* Space Observatory (Merín et al. 2008), and a proper motion study of these objects was performed by López Martí et al. (2011).

The focus of most kinematic studies over the past century was not the Lupus clouds, but the adjacent Scorpius-Centaurus (Sco-Cen) association that contains the nearest OB association. It is divided into the three subgroups Upper Scorpius (US), Upper Centaurus-Lupus (UCL) and Lower Centaurus-Crux (LCC). The Lupus molecular clouds, which are probably signposts of a more recent episode of star formation in that region (see Comerón 2008), occupy a gap between US and UCL. The distance of the Sco-Cen subgroups was investigated by de Zeeuw et al.

(1999), who assessed association membership again using the HIPPARCOS data and derived a mean distance of 140 pc for the UCL subgroup. The Lupus SFR was first estimated to be at the same distance as UCL (Hughes et al. 1993). The close proximity of the UCL subgroup makes it difficult to distinguish between members of the Lupus association and of the UCL association. Mamajek et al. (2002) conducted a spectroscopic survey of UCL candidate members and selected 56 stars that had the same proper motion as UCL association members. A more complete list containing 81 UCL candidate stars is given in the recent review on the Sco-Cen association by Preibisch & Mamajek (2008). As it turned out, many of these stars were previously reported as WTTs members of the Lupus association by Krautter et al. (1997) and Wichmann et al. (1997a,b). Since the membership status of these objects remains unclear, a more detailed study is clearly necessary.

In the past decade, several works have cast doubt on the distance to the Lupus star-forming region. From the angular extent of the molecular clouds (about 15 deg), and by assuming that the depth of the molecular region is comparable, the distances of individual association members are expected to range from about 110 pc to 190 pc. Two bright TTSs observed by HIPPARCOS, RY Lup, and V856 Sco are apparently associated with clouds of the Lupus star-forming region, and their parallaxes are compatible with the above range, but the cloud distances reported in the literature range from 100 pc (Knude & Hog 1998) to 360 pc for Lupus 2 (Knude & Nielsen 2001).

Bertout et al. (1999) used five stars connected with the Lupus complex that had been observed by HIPPARCOS to compute the average parallax of the Lupus SFR. They found a distance equal to 206^{+34}_{-20} pc, which is a high value compared to the previous estimates, but noticed that the group parallax determination was dominated by the brightest stars HIP 79080 and 79081, two components of a Herbig Ae/Be (HAeBe) system located in Lupus 3. Considering only the three fainter stars HIP 77157, 78094, and 78317, located in Lupus 1, 2, and 4, respectively, they obtained a distance of 147^{+42}_{-27} pc, in agreement with previous determinations of the Lupus association distance, but with a large uncertainty, and a value of 228^{+42}_{-30} pc for HIP 79080 and 79081. Bertout et al. (1999) concluded that either HIP 79080 and 79081 are not members of Lupus 3, which appears unlikely, or that this cloud is farther away than the other subgroups. Lombardi et al. (2008) conclude from their detailed study of 2MASS extinction maps that Lupus has a depth of 51^{+61}_{-35} pc and that this “*might be the result of different Lupus subclouds being at different distances*”. The kinematic study presented hereafter aims to shed light on the structure of the Lupus clouds, as well as on the membership of the Lupus association of PMS stars.

3. Sample of Lupus candidate members with known proper motions

3.1. Proper motions properties

The Ducourant et al. (2005, hereafter D05) proper motion catalog for PMS stars contains 197 stars in the general area of the Lupus SFR, which approximately ranges from $325^\circ \leq l \leq 342^\circ$ in Galactic longitude and $0^\circ \leq b \leq 25^\circ$ in Galactic latitude. The stars listed in this catalog were mostly identified by Herbig & Bell (1988), Krautter et al. (1997), and Wichmann et al. (1997a,b). We then included in the sample 37 stars of the comprehensive review performed by Comerón (2008) that were not considered in D05, and another 24 stars from the *c2d Spitzer* Legacy Program detected in the recent paper of López Martí

et al. (2011, only group A sources of their study). Our first list of presumed members of the Lupus association therefore consists of 258 stars.

To access the more recent measurements, we searched for proper motion data in the PPMXL (Roeser et al. 2010), SPM4 (Girard et al. 2011), and UCAC4 (Zacharias et al. 2012) catalogs for all the 258 stars in our sample. The main source of proper motions is the SPM4 catalog, which represents the best present-day compromise between proper motion precision and target coverage for the stars in our sample. For the brightest stars ($V \leq 12$) in the sample we also searched the TYCHO2 (Høg et al. 2000) catalog and used these values when the proper motions given in SPM4 were of lower precision. Doing so, we found proper motion information for 241 stars in our initial sample, and for the remaining ones we kept the proper motions given in D05. We used the proper motions of the PPMXL and UCAC4 catalogs for two stars, since these are the only values available in the literature.

Whenever dealing with the kinematics of SFRs, the high fraction of binaries and multiple systems plays an important role. The overall binary fraction in Lupus is expected to reach about 30% to 40% (Ghez et al. 1997; Merín et al. 2008). An advantage of the D05 catalog is that these systems are clearly identified with a mention AB indicating that the given proper motion is representative of the binary system. In these cases we decided to use the proper motion given in D05 for both resolved and unresolved binaries rather than taking the value provided by SPM4, where the existence of close companions is not mentioned.

The CP search method selects cluster members and defines the CP of a moving group based on proper motion data. Therefore, before starting our analysis, it is necessary to reject all stars with proper motion that carry poor information because of measurement errors. From the sample we reject 33 stars whose proper motion is dominated by errors (i.e., $\sigma_{\mu_{\alpha,\delta}} \geq \mu_{\alpha,\delta}$) in both components. After a 3σ elimination in both proper motion components we reject another eight stars that are in obvious disagreement with the common streaming motion of the Lupus moving group. These stars are given in Table 1. The remaining 217 PMS stars will be used in this paper to investigate the kinematic properties of this SFR and discuss their membership status based on the CP analysis. Their average proper motion is $(\mu_{\alpha} \cos \delta, \mu_{\delta}) = (-16, -21)$ mas/yr with an average precision of about 2 mas/yr in each component.

Figure 1 displays all proper motion values and their associated uncertainties. We note that a small group of these stars displays small proper motions. Because we considered only stars related to the Lupus SFR whose PMS status had already been established in previous works, it appears unlikely that field stars pollute our sample. We therefore assume for the moment that these stars form a background population belonging to the Lupus complex, and we come back to this point in Sect. 7. Figure 2 shows the proper motion vectors for our sample of Lupus stars. Although the position of the CP is not clearly apparent in this plot, one notices that most proper motion vectors point in a common direction. The precise coordinates of the CP will be derived in Sect. 5.

3.2. Refining the Lupus pre-main sequence star sample

While the majority of the stars in our sample lie very close to the Lupus clouds, a fraction of the stars are scattered over a wider region (see Fig. 3). Most of these stars were identified and classified as WTTSSs by Krautter et al. (1997) and Wichmann et al. (1997a,b) from ROSAT X-ray pointed observations and the

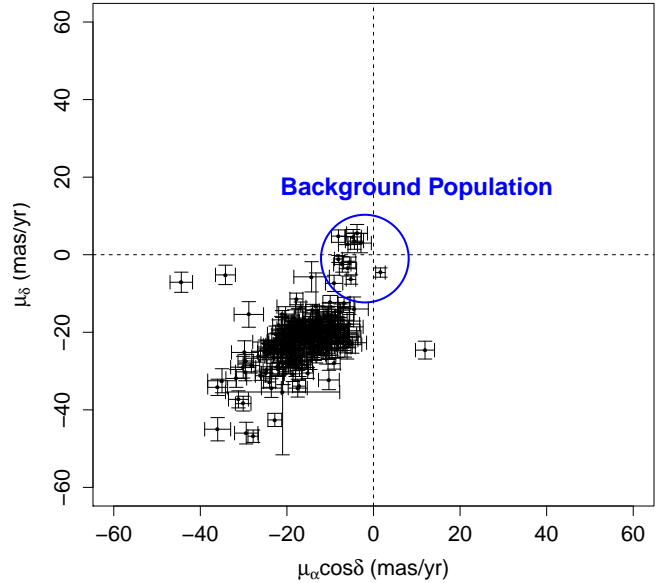


Fig. 1. Proper motion and associated errors for the 217 stars considered in this work.

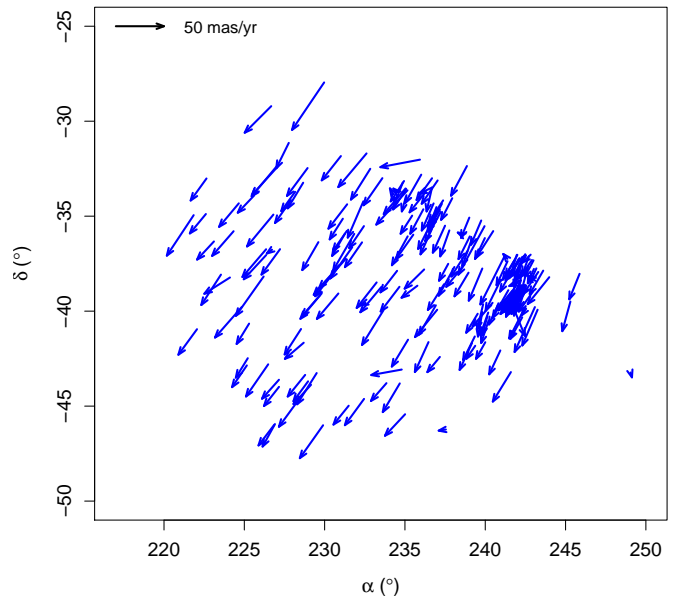


Fig. 2. Proper motion vectors of the 217 Lupus candidate stars.

ROSAT All Sky Survey (RASS). However, we mentioned that the Lupus SFR is located near the UCL subgroup of the Sco-Cen association, so one suspects that some of these stars might not be related to the Lupus SFR but might instead be part of the older Sco-Cen association. Indeed, a list of 81 low-mass candidate members of the UCL subgroup is given in the review by Preibisch & Mamajek (2008), and our sample of Lupus association candidate members includes 25 stars of their list. Preibisch

Table 1. Rejected stars from our sample of Lupus candidate members.

Star	α (h:m:s)	δ ($^{\circ}$ ' '')	$\mu_{\alpha} \cos \delta$ (mas/yr)	μ_{δ} (mas/yr)	Source	2MASSJ
RXJ1508.4-3337	15 08 26.2	-33 37 52	$+21.0 \pm 14.0$	$+16.0 \pm 14.0$	D05	15082621-3337517
RXJ1514.0-4629B	15 13 59.8	-46 29 54	$+29.0 \pm 13.0$	$+18.0 \pm 13.0$	D05	15135984-4629540
HD137727	15 28 44.0	-31 17 38	$+19.9 \pm 2.0$	$+48.0 \pm 1.9$	TYCHO2	15284402-3117387
Sz66	15 39 28.3	-34 46 18	$+160.3 \pm 5.4$	-40.8 ± 5.4	UCAC4	15392828-3446180
HD140637	15 45 47.6	-30 20 55	-70.7 ± 2.4	-96.4 ± 2.8	SPM4	15454761-3020555
Sz101	16 08 28.4	-39 05 32	$+88.8 \pm 3.9$	$+29.1 \pm 4.0$	SPM4	16082843-3905324
RXJ1609.3-3855AB	16 09 23.2	-38 55 55	$+93.0 \pm 14.0$	-119.0 ± 14.0	D05	16092320-3855547
V346Nor	16 32 32.1	-44 55 31	$+63.0 \pm 17.0$	$+130.0 \pm 17.0$	D05	16323219-4455306

Notes. We provide the most usual identifier, position (epoch 2000), proper motion, source of proper motion, and the 2MASS identifier for each star.

& Mamajek (2008) also claim that other stars previously identified as Lupus PMS stars by Krautter et al. (1997) and Wichmann et al. (1997b) appear to be UCL members because of their proper motions and positions in the HR-diagram.

It appears (Preibisch & Mamajek 2008) that the UCL stars are spread over a large extent on the sky, while the spatial distribution of Lupus stars exhibits two components: (i) an *on-cloud* population concentrated in the immediate vicinity of the molecular clouds and (ii) a more dispersed *off-cloud* population surrounding the clouds. The corresponding region spans the range of Galactic coordinates $334^{\circ} \leq l \leq 342^{\circ}$ and $5^{\circ} \leq b \leq 25^{\circ}$ and contains 160 stars, while the off-cloud population in our sample is located in the region with $l < 334^{\circ}$, which contains 57 stars. There is some arbitrariness involved in defining these regions, but the idea of separating our sample into two groups turned out to be necessary to our analysis, as is seen below, and has also been suggested by Preibisch & Mamajek (2008), who wrote “... it is probably wise for astrophysical studies to separate the *on- or near-cloud Lupus members from the off-cloud UCL/US members*.”. We show that the off-cloud population is indeed a mix of Lupus and UCL stars in Sect. 5.

In Table 2 we present the median positions, proper motions, and radial velocities for the Lupus subgroups. We find good agreement between the proper motions of the various star-forming clouds (Lupus 1 - 4). When comparing the proper motions of on-cloud and off-cloud stars, we note a difference of about 7 mas/yr in right ascension, although the median values for both populations are perfectly compatible in declination. One possibility to explain this difference is the existence of field stars or UCL members in the off-cloud sample as mentioned before. However, the reported difference of 7 mas/yr is still consistent e.g. with the observed extreme proper motion values for the various subgroups of the Taurus complex where a single UVW velocity value can be adopted assuming a velocity dispersion of about 1 km/s among the different subgroups (see Luhman et al. 2009). In the case of radial velocities, we consider both radial velocities from the literature and additional measurements derived in this paper (to be discussed in Sect. 4). Binaries and stars with insignificant measurements (i.e., $\sigma_{V_r} \geq V_r$) are excluded from the analysis presented in Table 2. We note that stars in the off-cloud region exhibit radial velocities that are slightly higher than the values observed for the on-cloud population, which can be explained by geometrical effects, because both populations are at different angular separations from the CP. In the following, we assume that the Lupus stars spread over the various subgroups are comoving and use the CP search method to identify a moving group of PMS stars in this SFR.

4. Radial velocities

We mentioned that stellar radial velocities (RVs) are needed to determine individual parallaxes. We summarize here our search for RVs in the literature and some additional observations for stars with unknown RVs.

4.1. Radial velocities from the literature

We searched the CDS databases to access RV information for the stars in our sample. The search made use of the data mining tools available on the CDS site. We also looked for published RV data that are not available via the web-based CDS service. Our search for RVs, made as exhaustive as possible, is based on Herbig & Bell (1988), Gregorio-Hetem et al. (1992), Barbier-Brossat et al. (1994), Duflo et al. (1995), Dubath et al. (1996), Grenier et al. (1999), Wichmann et al. (1999), Barbier-Brossat & Figon (2000), Madsen et al. (2002), Melo (2003), Nordström et al. (2004), Bobylev (2006), Gontcharov (2006), James et al. (2006), Malaroda et al. (2006), Torres et al. (2006), Guenther et al. (2007), Kharchenko et al. (2007), and White et al. (2007).

We found RVs for only 108 stars of the full sample (on-cloud and off-cloud populations), which reflects the scarcity of this measurement in the literature. This is because previous spectroscopic investigations in Lupus have often focused on the few bright stars of this region. Figure 4 displays the RV distribution in our sample.

4.2. Additional radial velocity observations

The scarcity of measured RVs is the main limitation in deriving individual distances in this work. To increase the number of Lupus stars with known RV information, we thus performed spectroscopic observations with the high-resolution ($R = 48000$) FEROS (Kaufer et al. 1999) échelle spectrograph mounted at the ESO/MPG 2.2m telescope operated at La Silla (Chile). In addition to its high performance, FEROS provides a full wavelength coverage in the optical region (between 3500Å and 9200Å) over 39 spectral orders. The observations were taken in object calibration mode, which allows acquiring simultaneous spectra of the object and of the ThAr cell. Exposure times ranged from 5 min to 60 min, so that a S/N of about 20-30 was achieved. We observed 52 stars spread over the Lupus and Ophiuchus¹ SFRs during the

¹ The kinematic properties of the Ophiuchus SFR will be presented in a companion paper (Galli et al., in preparation). However, the results of our observations are presented in this paper since only a few stars of that region were observed in our program.

Table 2. Median positions, proper motions, radial velocities, and the number of stars for the various subgroups in Lupus.

Sample	α (h:m:s)	δ ($^{\circ}$ ' '')	l ($^{\circ}$)	b ($^{\circ}$)	$\mu_{\alpha} \cos \delta$ (mas/yr)	μ_{δ} (mas/yr)	V_r (km/s)	Stars
Lupus 1	15 46 42.1	-35 00 46	338.8	15.3	-14.0	-21.1	2.5 ± 1.6	30
Lupus 2	15 56 02.1	-37 56 06	338.6	12.0	-15.0	-23.1	2.2 ± 0.9	15
Lupus 3	16 08 53.2	-39 05 34	339.5	9.4	-12.0	-20.4	1.0 ± 0.7	73
Lupus 4	15 59 16.5	-41 57 10	336.2	8.5	-10.0	-20.8	0.3 ± 3.8^a	9
Lupus (on-cloud)	16 00 47.0	-38 48 54	339.1	9.7	-13.0	-21.6	2.5 ± 0.4	160 ^b
Lupus (off-cloud)	15 12 39.8	-40 50 52	329.9	14.0	-20.0	-21.8	4.6 ± 0.4	57
Lupus (full sample)	15 49 30.7	-38 59 48	338.2	11.0	-16.0	-21.7	3.7 ± 0.4	217

Notes. The uncertainties in the median proper motion values for each group are about 1-2 mas/yr.^(a) The radial velocity value presented for Lupus 4 is based on only two stars and should be regarded with caution. ^(b) The number of stars in the Lupus star-forming clouds (Lupus 1 - 4) do not add to the total number of stars (160 stars) in the on-cloud population (see definition in Sect. 3.2), because those stars that are spread beyond the limits of these clouds (see ^{12}CO intensity map in Fig. 3) were not assigned to any cloud.

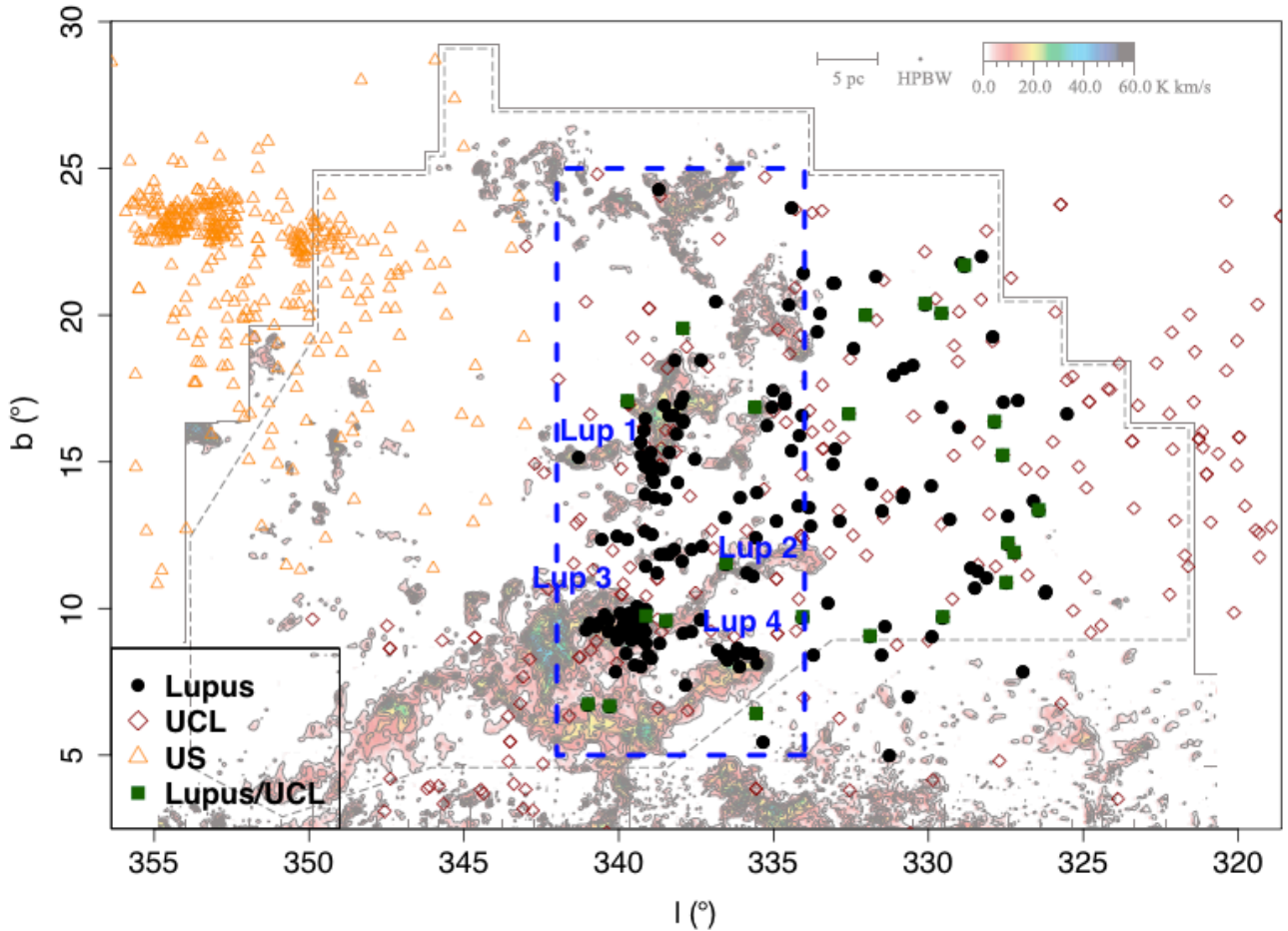


Fig. 3. Location of the 217 Lupus PMS stars overlaid on the ^{12}CO intensity map from Tachihara et al. (2001). Stars from US and UCL subgroups of the Sco-Cen association as given in de Zeeuw et al. (1999) and Preibisch & Mamajek (2008) are also included in this figure. Black filled circles denote the Lupus candidate stars and open symbols indicate US and UCL members. Stars marked with green filled squares were classified as both Lupus and UCL members in the literature. The blue dashed box encloses the Lupus star-forming clouds.

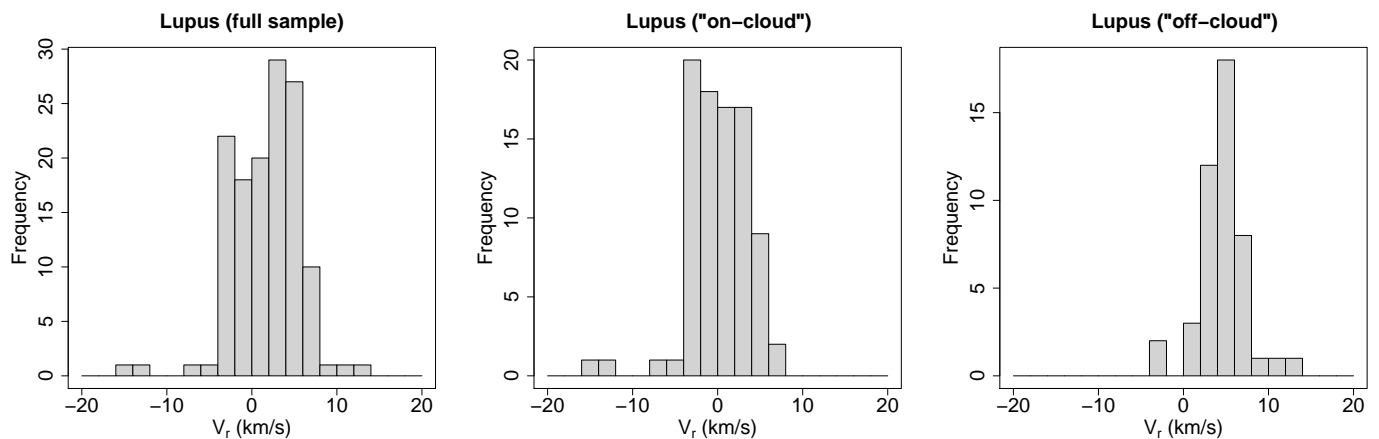


Fig. 4. Histogram of RVs found in the literature for Lupus stars.

nights of April 29 to May 05, 2011. Binaries and stars belonging to multiple systems as given in the literature were not included in our list of targets. The observed spectra were reduced with the standard FEROS data reduction pipeline, which performs bias subtraction, flat-fielding, scattered-light removal, échelle-order extraction, barycentric velocity correction, and wavelength calibration of the spectra. The extracted wavelength-calibrated spectra for each spectral order were not merged into a single spectrum, but used as 39 separate spectra (one per order) to determine the RV of the target. This procedure enabled us to eliminate the largest noise contributions that come from the orders in the red (orders ≤ 7) and blue (orders ≥ 30) regions of the spectra (see Setiawan et al. 2003).

We derived RVs by cross-correlating the reduced spectra of program stars with template spectra. To maximize the quality of our RV measurements we used both a standard-star spectrum and a numerical mask as template spectrum.

The cross-correlation with a stellar template utilized the standard star HD 82106 ($V = 7.2$ mag, K3V), which was observed every night and whose RV is known to a high accuracy ($V_r = +29.75 \pm 0.05$ km/s, Udry et al. 1999). We computed the RVs of program stars by cross-correlating their spectrograms order-by-order with one reference spectrogram of HD 82106 (taken on May 4, 2011) using the IRAF task *fxcor*. We obtained the RV for each order separately and then averaged these values. The errors of our RV measurements were determined from the variance of all orders considered. Orders with discrepant values (due to a lower S/N) were obviously not considered. To investigate the accuracy of our results we calculated the RV of HD 82106 as derived from our observations. We cross-correlated the reference spectrogram with all spectrograms of HD 82106 spread over the whole observing campaign. The absolute RV of the reference spectrum was determined by cross-correlating it with the solar spectrum. The mean RV derived from our observations is $V_r = +29.71 \pm 0.05$ km/s, in good accordance with Udry et al. (1999).

The other alternative to computing RVs consisted of a cross-correlation with a box-shaped binary template. The procedure follows the method outlined in Baranne et al. (1996), which fits a Gaussian to the cross-correlation function of each order. The center of the Gaussian then gives the RV of the target (see Weise et al. 2010, for more details). To better compare the RVs derived for HD 82106 using both techniques, we used a binary template of a G2V star. Our choice of the template was motivated by the

use of the solar spectrum to derive the absolute RV of HD 82106 in our first approach (see above). For program stars, we used a K0V star template that is more representative of our targets' spectral types. The mean RV derived with this alternative strategy is $V_r = +29.74 \pm 0.04$ km/s, which is perfectly consistent with the values mentioned above.

Using both a standard-star spectrum and a numerical template is valuable for gaining confidence in the derived results. To spot possible errors, the RVs of program stars were computed using only the common (not rejected) orders in both procedures. The final RV of our targets is the average of two independent values (one for each method). The uncertainties are calculated by propagating the individual errors and they are of a few hundred m/s. When one of the methods failed to return a RV value (due to low S/N in some orders) we only considered the result derived by the other method. A more realistic idea of our external precision is given in Table 3 by comparing the RVs derived in this work with published results for a control group of 3 stars in our sample with previously known RVs. We conclude that our results are fully compatible with the values found in the literature, with a rms uncertainty of about 500 m/s. We present the RVs of 52 stars belonging to the Lupus and Ophiuchus SFRs in Table 4, together with the Li I and H α equivalent widths (EWs) derived from our observations.

Table 3. Comparison of RVs derived in this paper with those published in the literature.

Star	This Work	Literature	Reference
	V_r (km/s)	V_r (km/s)	
RXJ1524.5-3652	3.75 ± 0.33	4.2 ± 1.0	Wichmann et al. (1999)
		4.1 ± 0.4	Torres et al. (2006)
		4.4 ± 0.4	James et al. (2006)
		4.6 ± 0.4	James et al. (2006)
RXJ1547.6-4018	2.85 ± 0.37	2.8 ± 1.0	Wichmann et al. (1999)
		3.2 ± 0.1	Torres et al. (2006)
		3.1 ± 0.4	James et al. (2006)
		3.2 ± 0.4	James et al. (2006)
RXJ1538.0-3807	2.46 ± 0.28	3.4 ± 1.0	Wichmann et al. (1999)
		3.0 ± 0.2	Guenther et al. (2007)

Equivalent widths of the Li I and H α lines were measured from our spectra using IRAF *splot* routine. The presence of Li absorption in late-type stars is one of the primary criteria for stellar youth (see Basri et al. 1991). The Li I $\lambda 6708\text{\AA}$ resonance

Table 4. Results from our observations.

Star	α (h:m:s)	δ ($^{\circ}$ ' '')	V_r (km/s)	$EW(Li)$ (\AA)	$EW(H\alpha)$ (\AA)	Remarks
<i>Lupus</i>						
RXJ1448.2-4103	14 48 13.3	-41 02 58	$+5.95 \pm 0.17$	0.336 ± 0.017	≤ 0.1	WTTS
RXJ1452.4-3740	14 52 26.2	-37 40 08	$+5.00 \pm 0.40$	0.402 ± 0.003	≤ 0.1	WTTS
RXJ1454.2-3955	14 54 11.3	-39 55 23	$+3.83 \pm 0.38$	0.382 ± 0.002	-0.68 ± 0.04	WTTS
RXJ1502.4-3405	15 02 26.0	-34 05 13	$+3.88 \pm 0.17$	0.437 ± 0.001	-0.27 ± 0.08	WTTS
RXJ1505.4-3857	15 05 25.9	-38 57 03	$+4.92 \pm 0.33$	0.416 ± 0.004	-0.92 ± 0.08	WTTS
RXJ1505.9-4311	15 05 56.9	-43 12 02	$+3.99 \pm 0.27$	0.465 ± 0.001	-0.99 ± 0.05	WTTS
RXJ1506.7-3047	15 06 42.6	-30 47 33	$+0.81 \pm 0.24$	0.480 ± 0.002	-1.82 ± 0.13	WTTS
RXJ1508.0-3338	15 08 05.1	-33 37 55	$+1.65 \pm 0.23$	0.447 ± 0.010	-0.55 ± 0.02	WTTS
RXJ1508.4-3338	15 08 25.0	-33 37 55	$+1.85 \pm 0.43$	0.438 ± 0.011	-1.29 ± 0.11	WTTS
RXJ1508.8-3715	15 08 53.8	-37 15 46	$+4.51 \pm 0.28$	0.421 ± 0.012	-0.50 ± 0.06	WTTS
RXJ1515.1-4438	15 15 09.3	-44 38 36	$+6.34 \pm 0.34$	0.367 ± 0.012	-1.11 ± 0.05	WTTS
RXJ1518.0-4445	15 18 01.3	-44 44 26	$+5.97 \pm 0.15$	0.099 ± 0.007	0.81 ± 0.05	WTTS
RXJ1524.5-3652	15 24 32.4	-36 52 02	$+3.75 \pm 0.33$	0.344 ± 0.001	≤ 0.1	WTTS
RXJ1526.8-3721	15 26 52.6	-37 22 06	$+1.92 \pm 0.21$	0.505 ± 0.002	-2.25 ± 0.15	WTTS
RXJ1529.8-4523	15 29 48.9	-45 22 45	$+4.64 \pm 0.41$	0.442 ± 0.008	-0.75 ± 0.03	WTTS
RXJ1534.3-3300	15 34 23.2	-33 00 09	$+1.40 \pm 0.20$	0.525 ± 0.008	-1.11 ± 0.08	WTTS
RXJ1538.0-3807	15 38 02.7	-38 07 23	$+2.46 \pm 0.28$	0.423 ± 0.021	-1.93 ± 0.44	WTTS
RXJ1539.7-3450	15 39 46.4	-34 51 02	$+5.39 \pm 0.29$	0.284 ± 0.013	-0.32 ± 0.02	WTTS
RXJ1542.0-3601	15 42 05.2	-36 01 32	-0.05 ± 0.26	0.492 ± 0.011	-0.81 ± 0.03	WTTS
RXJ1544.5-3521	15 44 35.3	-35 21 49	$+2.47 \pm 0.23$	0.491 ± 0.008	-1.37 ± 0.07	WTTS
RXJ1547.1-3540	15 47 08.4	-35 40 19	$+0.82 \pm 4.90$	0.472 ± 0.016	-1.09 ± 0.39	WTTS
RXJ1547.6-4018	15 47 41.8	-40 18 26	$+2.85 \pm 0.37$	0.387 ± 0.012	0.17 ± 0.01	WTTS
RXJ1548.0-4004	15 48 02.1	-40 04 28	$+2.07 \pm 0.35$	0.433 ± 0.014	-2.01 ± 0.06	WTTS
RXJ1548.9-3513	15 48 54.1	-35 13 18	$+0.62 \pm 0.16$	0.372 ± 0.002	-0.41 ± 0.03	WTTS
RXJ1601.8-4026	16 01 49.5	-40 26 19	$+2.87 \pm 0.46$	0.371 ± 0.011	-1.39 ± 0.08	WTTS
RXJ1606.3-4447	16 06 23.4	-44 47 35	$+4.68 \pm 0.54$	0.455 ± 0.007	-0.48 ± 0.06	WTTS
RXJ1608.0-3857	16 08 00.0	-38 57 51	-2.42 ± 0.84	0.638 ± 0.002	-1.91 ± 0.14	WTTS
F304	16 08 11.0	-39 10 46	$+2.76 \pm 0.11$	0.449 ± 0.001	-0.66 ± 0.02	WTTS
V908Sco	16 09 01.9	-39 05 12	-0.77 ± 0.82	0.570 ± 0.004	-51.24 ± 4.20	CTTS
RXJ1609.9-3923	16 09 54.0	-39 23 27	-0.21 ± 0.46	0.550 ± 0.003	-22.33 ± 0.93	CTTS
RXJ1611.6-3841	16 11 38.0	-38 41 35	$+2.52 \pm 0.39$	0.438 ± 0.007	-3.93 ± 0.31	WTTS
RXJ1615.9-3947	16 15 56.7	-39 47 16	$+0.09 \pm 0.27$	0.456 ± 0.011	-2.37 ± 0.23	WTTS
RXJ1615.9-3241	16 15 57.0	-32 41 24	-0.45 ± 0.26	0.458 ± 0.010	-0.68 ± 0.06	WTTS
HD147454	16 23 32.3	-34 39 50	-0.10 ± 0.41	0.112 ± 0.004	2.32 ± 0.15	WTTS
SAO207620	16 23 37.7	-34 40 21	-0.41 ± 0.14	0.195 ± 0.005	0.72 ± 0.09	WTTS
<i>Ophiuchus</i>						
GSC6780-1061	16 06 54.4	-24 16 11	-5.43 ± 0.19	0.561 ± 0.001	-1.55 ± 0.09	WTTS
GSC6793-994	16 14 02.1	-23 01 02	-2.28 ± 0.51	0.356 ± 0.013	≤ 0.1	WTTS
PDS145	16 14 20.9	-19 06 05	-7.67 ± 10.85	0.261 ± 0.007	-65.94 ± 2.30	CTTS
RXJ1620.7-2348	16 20 46.0	-23 48 21	-3.21 ± 0.21	0.465 ± 0.002	-0.37 ± 0.07	WTTS
RXJ1621.4-2312	16 21 28.5	-23 12 11	-8.37 ± 2.24	0.588 ± 0.011	-1.27 ± 0.09	WTTS
Harol-1	16 21 34.7	-26 12 27	-4.29 ± 0.50	0.455 ± 0.024	-153.60 ± 2.50	CTTS
GSC6794-537	16 23 07.8	-23 01 00	-10.05 ± 1.41	0.491 ± 0.011	-0.52 ± 0.10	WTTS
GSC6794-156	16 24 51.4	-22 39 32	-5.27 ± 1.72	0.338 ± 0.001	-0.90 ± 0.18	WTTS
RXJ1625.4-2346	16 25 28.6	-23 46 27	-10.38 ± 0.64	0.381 ± 0.001	0.24 ± 0.01	WTTS
DoAr25	16 26 23.7	-24 43 14	-8.25 ± 0.59	0.547 ± 0.002	-8.28 ± 0.50	CTTS
RNO90	16 34 09.2	-15 48 17	-12.92 ± 7.92	0.360 ± 0.006	-78.00 ± 2.40	CTTS
He3-1254	16 46 44.3	-15 14 38	-8.98 ± 0.29	0.444 ± 0.008	-97.14 ± 4.40	CTTS
WaOph6	16 48 45.6	-14 16 36	-10.09 ± 0.54	0.520 ± 0.009	-24.19 ± 0.95	CTTS
WaOph5	16 49 00.8	-14 17 11	-9.54 ± 3.04	0.668 ± 0.001	-54.07 ± 7.31	CTTS
V1725Oph	17 16 13.9	-20 57 46	-11.77 ± 0.84	0.636 ± 0.007	-22.51 ± 1.60	CTTS
GSC6213-194	16 09 41.0	-22 17 59				SB2, WTTS
RXJ1613.1-3804	16 13 12.7	-38 03 51				SB2, WTTS

Notes. The upper panels present the RVs derived in this paper, together with EWs for the Li and $H\alpha$ lines. We also provide the TTS subclass based on $EW(H\alpha)$. The symbol “:” indicates uncertain values of RVs where one of the cross-correlation techniques failed to return a result. Negative and positive values of $EW(H\alpha)$ denote that the line is in emission and absorption, respectively. The lower panel presents those stars that show evidence of spectroscopic binarity (SB2).

doublet is blended by Fe lines and the lithium isotope ${}^6\text{Li}$. It is not possible to separate individual lines at our spectral resolution (~ 48000), so we see no evidence of these features. The lithium EWs were measured using both a Gaussian fit and direct integration. The difference between these values is smaller than $25 \text{ m}\text{\AA}$, which we consider to be the upper limit of our measurement errors. The contribution from the neighboring blending lines is expected to be smaller than the uncertainty of our results, which we estimated by varying the location of the continuum adjacent to the line.

The $\text{H}\alpha$ emission line is one the most prominent spectroscopic features in the visible spectra of CTTs (Joy 1945; Herbig 1962). The line profile is often complex and takes different shapes, which were studied and classified by Reipurth et al. (1996). We measured the $\text{H}\alpha$ EWs by direct integration and by fitting a Voigt profile (when the target exhibited a $\text{H}\alpha$ profile with a single peak). Our measurement errors are mainly caused by the uncertainty on the continuum level in the vicinity of the line. We use the standard limit of 10\AA (see, e.g., Appenzeller & Mundt 1989) to distinguish between CTTs ($\text{EW}(\text{H}\alpha) \geq 10\text{\AA}$) and WTTs ($\text{EW}(\text{H}\alpha) < 10\text{\AA}$) and find that our sample contains 10 CTTs and 42 WTTs. A more detailed inspection of the spectra in our sample revealed two PMS spectroscopic binaries (SB2), for which no evidence of binarity could be found in the literature prior to our observations. We present the results of our observations in Table 4.

5. Analysis and results

In the following we derive the CP of the comoving group of Lupus stars considered in this paper. We first use the k -nearest neighbor (k -NN, Fix & Hodges 1951; Venables & Ripley 2002) algorithm to distinguish between Lupus and UCL stars based on their position, then we apply the CP search method to the sample of Lupus candidate members and perform a membership analysis. The technique that we use to find the CP position of the Lupus moving group is the new CP search method that was recently developed by our team. We refer the reader to the original paper (Galli et al. 2012) for more details on the implementation of this method.

5.1. Preliminary analysis

The velocity dispersion in Lupus is a first input parameter that we must determine for performing the CP analysis. The velocity dispersion of young moving groups is expected to be low, only a few km/s (Mathieu 1986). Typical values of velocity dispersion in nearby SFRs are 1-2 km/s (Jones & Herbig 1979; Dubath et al. 1996; Makarov 2007; Luhman et al. 2009). We adopt $\sigma_v = 1 \text{ km/s}$ as the one-dimensional velocity dispersion of the Lupus moving group, and we come back to this point in Sect. 6. Another input parameter in the CP method is the mean distance to the moving group. As discussed in Sect. 2, the distance to the Lupus SFR has undergone substantial revision in the literature over the past decade. Here we use the value of $d = 150 \text{ pc}$ that seems to be adequate for most of the clouds in the complex (Comerón 2008). The CP search method is rather insensitive to small variations in both parameters.

When we apply the CP search method to the 217 stars in the sample, we end up with a CP position given by

$$(\alpha_{cp}, \delta_{cp}) = (93.3^\circ, -25.7^\circ) \pm (1.8^\circ, 2.6^\circ)$$

with 125 moving group members. In a recent paper, Makarov (2007) investigated the kinematics of the Lupus sample of 93 PMS stars identified by Krautter et al. (1997) using the UCAC2 catalog (Zacharias et al. 2004) and derived a velocity dispersion of 1.3 km/s . The CP position presented in his work is $(\alpha_{cp}, \delta_{cp}) = (92.8^\circ, -28.1^\circ) \pm (3.1^\circ, 5.0^\circ)$.

We note that there is good agreement between both solutions, and it is probable that the small differences are caused by the different samples of Lupus stars, the different proper motion sources, and the different CP search methods. However, whether the above result is the most appropriate for the sample of TTs associated with the Lupus molecular clouds is questionable since the derived CP solution might be affected by UCL stars misidentified as Lupus WTTs. We investigate this question below.

5.2. The k -NN algorithm applied to the sample of Lupus stars

The k -NN method is a nonparametric machine learning algorithm used in pattern recognition for classifying objects. Although the k -NN method is not yet widely used in astronomy, it has already proven to be effective, such as for the photometric search of brown dwarfs (Marengo & Sanchez 2009) and estimations of photometric redshifts for quasars (Ball et al. 2007). It is used in this work to segregate potential Lupus and UCL members in our *test sample* of 217 stars based on their position with respect to both the star-forming clouds and confirmed members of each association.

In the classic version of the k -NN method, a test element is classified by the majority vote of its k nearest neighbors from the *training set*. To begin with, we define the training set $T = \{(\mathbf{x}_1, y_1), (\mathbf{x}_2, y_2), \dots, (\mathbf{x}_N, y_N)\}$, where \mathbf{x}_i is the vector of attributes (stellar positions), $\mathbf{x}_i = (\alpha_i, \delta_i)$, and $y_i \in \{c_1, c_2\}$ denote the class membership (Lupus or UCL). The training set used in this work includes both Lupus and UCL stars, and it is constructed as follows. Since most members of the Lupus SFR are already included in our test sample (and many of them lack membership confirmation) we use the position of the 105 molecular clouds detected in ${}^{12}\text{CO}$ by Tachihara et al. (2001) for this purpose, and the 81 stars given by Preibisch & Mamajek (2008) as UCL members.² Stars in our test sample are classified as potential Lupus or UCL members based on the majority vote of their k nearest neighbors where the value of k is optimized to our specific problem (see below). In this context, the probability $p(y | x)$ for a given star with attributes (\mathbf{x}, y) is given by

$$p(y = c | x) = \frac{k_c}{k} \quad (1)$$

where k_c denotes the number of nearest neighbors in the training set labeled with class c (Lupus or UCL).

One important point to be considered in the k -NN algorithm is the best choice of k . While higher values of k would make the boundaries between Lupus and UCL less clear, a low value, on the other hand, can lead to noisy classification. An odd number for k is preferable and avoids tied votes since we only have to distinguish between two classes. To gain confidence in the derived results and determine the optimum value for k , we construct a

² Although a larger sample of UCL members from the HIPPARCOS catalog exists (see e.g. de Zeeuw et al. 1999), we prefer at this stage to use only those provided by Preibisch & Mamajek (2008) in order to keep approximately the same fraction of Lupus and UCL data points in the training set to avoid a classification bias. The remaining UCL stars will be used later in this section to investigate the accuracy of our procedure and determine the optimum value of k (see text).

total of 1000 synthetic test samples to be classified by the k-NN method using the procedure described above. To do so, we use the well-known UCL members from the HIPPARCOS catalog given by de Zeeuw et al. (1999), and simulate synthetic Lupus training stars by generating stellar positions from a Gaussian distribution using the position of the ^{12}CO -peak-integrated intensity and the radius of the molecular clouds as given in Table 1 of Tachihara et al. (2001). At each run our routine randomly chooses Lupus and UCL test stars to construct samples with 200 stars and classify them based on our training set. The fraction of Lupus and UCL stars in the synthetic test samples is not fixed and varies at each iteration to avoid any bias when evaluating the accuracy of the procedure.

The first results of our simulations, however, revealed that many Lupus synthetic stars located in the core of the star-forming clouds were misclassified. This is because some data points in our training set refer to single stars, while others in principle represent the center position of molecular clouds. Neither the size of the molecular clouds nor the distance to nearer neighbors are taken into account, showing that the majority vote criteria is not suited to our specific case. One way to solve this problem is to not give the same weight (vote) to all the neighbors. In this context, we implement a *weighted k-NN algorithm* that uses a distance weighted function. We distinguish whether the positions (α_i, δ_i) in the training set refer to molecular clouds (Lupus) or stars (UCL) by assigning a different weight. The weight function ω_i is given by

$$\omega_i = \begin{cases} 1/(d-r), & \text{molecular cloud} \\ 1/d, & \text{star} \end{cases}$$

where r is the radius of the molecular cloud and d is calculated from the position of the ^{12}CO -peak-integrated intensity of the Lupus molecular clouds (see Tachihara et al. 2001) or the position of the UCL star in the training set. The angular distance d between a test star with given position (α_j, δ_j) and a training star (α_i, δ_i) is given by

$$d = \cos^{-1}[\sin \delta_i \sin \delta_j + \cos \delta_i \cos \delta_j \cos(\alpha_i - \alpha_j)]. \quad (2)$$

In this case the posterior probability for a given star in the test sample takes the weight function into account and it is defined as

$$p(y = c | x) = \frac{\sum_{i=1}^{k_c} \omega_i}{\sum_{i=1}^k \omega_i}, \quad (3)$$

where the sum in the numerator runs only over the nearest neighbors in the training set with class c (Lupus or UCL). We use these probabilities to classify the stars in our test sample as potential Lupus or UCL candidate members.

Figure 5 compares the performance of our refurbished weighted k-NN method with its classic version for various values of k . We conclude that our new strategy indeed yields better results and exhibits an accuracy of $\sim 80\%$. The accuracy is defined by the fraction of test stars in our simulated test samples that are correctly classified by the k-NN algorithm. We conclude that any value of k between 7 and 15 can be used in this work to segregate potential Lupus and UCL stars. We adopt $k = 15$ under the assumption that more neighbors will help better define both groups. Doing so, we run the weighted k-NN method in our original test sample of 217 stars and identify 183 stars as potential Lupus members and 34 stars as potential UCL members. The

distribution of Lupus and UCL stars is illustrated in Fig. 6 and shows that the majority of Lupus stars is located in the vicinity of the molecular clouds (as expected).

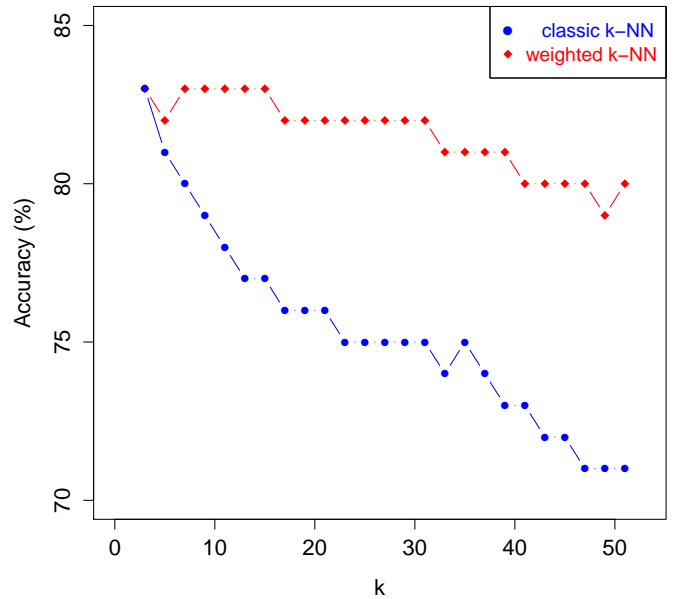


Fig. 5. Comparison of performance between the classic and weighted k-NN methods as a function of k derived from our simulations. Each point represents an average value of 1000 iterations.

5.3. Convergent point analysis for the Lupus moving group

The procedure described in the previous section made it possible to separate some potential UCL members included in our initial sample of Lupus PMS population. However, in order to search for association members, proper motions must be considered at this stage. Our final analysis consists in running the CP search method on the sample of 183 stars classified by the k-NN method as Lupus stars (see Sect. 5.2). We identify a moving group with 109 members and CP located at

$$(\alpha_{cp}, \delta_{cp}) = (112.2^\circ, -48.6^\circ) \pm (4.6^\circ, 3.6^\circ)$$

with chi-squared statistics $\chi_{red}^2 = 1.1$ (i.e., $\chi^2/\nu = 118.8/107$). We note that the rejection of some likely UCL members in our sample dramatically changed the CP position of the moving group as compared to our first solution in Sect. 5.1, which now appears to be a mixed CP solution of Lupus and UCL stars, and is therefore not valid for either moving group. Tables 5, 6, and 7 present the 109 Lupus moving group members selected by the CP search method, together with their parallaxes (to be discussed in Sect. 6). We note that six stars that were classified as UCL members by Preibisch & Mamajek (2008) and previously regarded as Lupus stars (Krautter et al. 1997; Wichmann et al. 1997a,b) have been accepted as Lupus members in our CP analysis. These stars are marked with the symbol “*”. On the other hand, we found that 19 stars previously regarded as WTTSs following their discovery in X-ray have been rejected in this analysis, and they are instead probable UCL members, as discussed by Preibisch & Mamajek (2008).

5.4. Result check via Monte Carlo simulations

To assess the validity of the CP location presented above, we performed Monte Carlo simulations of the 109 Lupus moving group members. We constructed 1000 samples of moving groups by re-sampling the stellar proper motions from a Gaussian distribution where the mean and variance are equal to the individual stellar proper motions and its uncertainty (in both components). We ran the CP search method for each set of simulated stars and computed the CP of each moving group. The results of this study are presented in Fig. 7. The CP solution derived in this paper is fully consistent with the centroid distribution of the Monte Carlo realizations, located at

$$(\alpha_{cp}, \delta_{cp}) = (112.6^\circ, -49.0^\circ) \pm (3.2^\circ, 2.5^\circ),$$

and we therefore conclude that it is representative of the Lupus moving group.

6. Kinematic parallaxes

6.1. Parallaxes and space velocities of group members with known radial velocity

Once the moving group is defined, it is possible to derive individual kinematic parallaxes π_{ind} for group members if their RVs V_r are known. Individual parallaxes are given by

$$\pi_{ind} = \frac{A \mu_{\parallel}}{V_r \tan \lambda}, \quad (4)$$

where $A = 4.74047$ km yr/s is the ratio of one astronomical unit in km to the number of seconds in one Julian year, λ is the angular distance from the CP position to a given star in the moving group, and μ_{\parallel} the stellar proper motion component that points towards the CP (see Galli et al. 2012, for more details). The parallax uncertainty is derived by error propagation of this equation and takes the error budget of proper motions, RVs, and the CP into account (see Appendix A for more details).

We found RVs for only 60 stars in the sample of 109 moving group members. We reject (resolved) binaries since it will not be possible to derive their parallaxes from a single RV measurement. Stars that exhibit poor RVs because of their errors are also excluded from this analysis. The observed RV for Lupus stars is expected to be low and a small variation accounts for a more significant shift in the parallax and space velocity (see Appendix B for more details). To spot possible errors on parallaxes and velocities, we define lower and upper limits for the space velocity of Lupus stars. To do so, we use five stars³ with known trigonometric parallax in the HIPPARCOS catalog that have been selected as moving group members in our CP analysis. The space velocities derived using HIPPARCOS parallaxes range from $V_{lower} \simeq 17$ km/s and $V_{upper} \simeq 33$ km/s, which define the limits for the space velocity of Lupus stars. This leaves us with a sample of 19 stars (see Table 5) that we define here as the Lupus *core moving group*. The mean parallax is $\bar{\pi} = 6.8 \pm 0.4$ mas, which agrees well with the estimated distance of 150 pc assumed in the CP analysis (see Sect. 5.1).

We computed the Galactic velocities for each star using the procedure described in Johnson & Soderblom (1987). Figure 8 displays the distribution of the UVW Galactic velocity components while Fig. 9 shows the velocity vectors of the 19 stars with

³ Sz 120 is not considered in this analysis because it is a binary HAeBe star (Correia et al. 2006).

individual parallaxes in a XYZ grid defined as follows. This reference system has its origin at the Sun where X points to the Galactic center, Y points in the direction of Galactic rotation, and Z points to the Galactic north pole.

The average space velocity for the Lupus moving group derived in this paper is

$$(U, V, W) = (-5.1, -20.7, -6.2) \pm (0.6, 1.1, 0.5) \text{ km/s},$$

$$V_{space} = 22.5 \pm 1.1 \text{ km/s}.$$

The space motion for the UCL subgroup was recently revised by Chen et al. (2011) to take into account the parallaxes from HIPPARCOS new reduction (van Leeuwen 2007) and modern RV compilations. They report a space velocity of $(U, V, W) = (-5.1, -19.7, -4.6) \pm (0.6, 0.4, 0.3)$ km/s. The relative space motion between Lupus stars and the UCL subgroup is $(\Delta U, \Delta V, \Delta W) = (0.0, -1.0, -1.6) \pm (0.8, 1.2, 0.6)$ km/s. These results suggest that Lupus is moving at 1.9 ± 1.6 km/s with respect to UCL and that their velocities are statistically indistinguishable at the 1-2 km/s level which roughly corresponds to the velocity dispersion in each group. A similar conclusion was reached regarding Ophiuchus stars and the US subgroup of the Sco-Cen association (see Mamajek 2008).

One particular point of the Lupus association is that the observed RVs of young stars are expected to be low and exhibit both positive and negative values (see e.g. Table 4 and Fig. 4). Among the moving group members with individual parallaxes presented in Table 5, a total of six stars exhibit negative values for their RVs. In such cases we use the absolute value of the RVs to compute the individual parallaxes using Eq. (4). In this context, Makarov (2007) reports a significant mismatch between the observed spectroscopic radial velocities and the value inferred from his CP solution, implying a moderate degree of expansion. That the Lupus association of young stars is undergoing expansion with a velocity of $\simeq 1$ km/s (see Makarov 2007) and the RVs are also near zero possibly explains the existence of the two RV populations. This situation contrasts with other SFRs, e.g. Taurus, where the observed RV is higher, $V_r \simeq +16$ km/s (see Luhman et al. 2009), and the existence of group members with RVs changing signs (i.e., $V_r < 0$) cannot be tolerated if assuming a one-dimensional velocity dispersion of only a few km/s.

When we run the CP search method on the sample of stars with known $V_r < 0$, we identify a moving group with 17 stars and CP located at $(\alpha_{cp}, \delta_{cp}) = (99.9^\circ, -36.1^\circ) \pm (7.3^\circ, 9.6^\circ)$. The large error bars in this CP solution arise from the small number of stars used for deriving the CP coordinates (see Galli et al. 2012). As one should notice, the effect of linear expansion changes the CP position (see also discussion in Makarov 2007), but the CP mentioned above is still compatible with the one given in Sect. 5.3. In the following we seek to learn whether the use of either CP solutions lead to significant differences in the derived parallaxes. We computed the individual parallaxes for those six stars again with $V_r < 0$ using the above mentioned CP and the procedure outlined in Appendix A. The average difference between the recomputed parallaxes and those given in Table 6 is $\Delta\pi = 0.3 \pm 0.1$ mas with rms of 1.1 mas, and they are statistically compatible within their error bars. The re-evaluated UVW velocity components for these stars has a negligible effect on the average space motion of the Lupus moving group, yielding instead

$$(U, V, W) = (-5.2, -20.9, -6.3) \pm (0.6, 1.0, 0.5) \text{ km/s},$$

$$V_{space} = 22.7 \pm 1.1 \text{ km/s}.$$

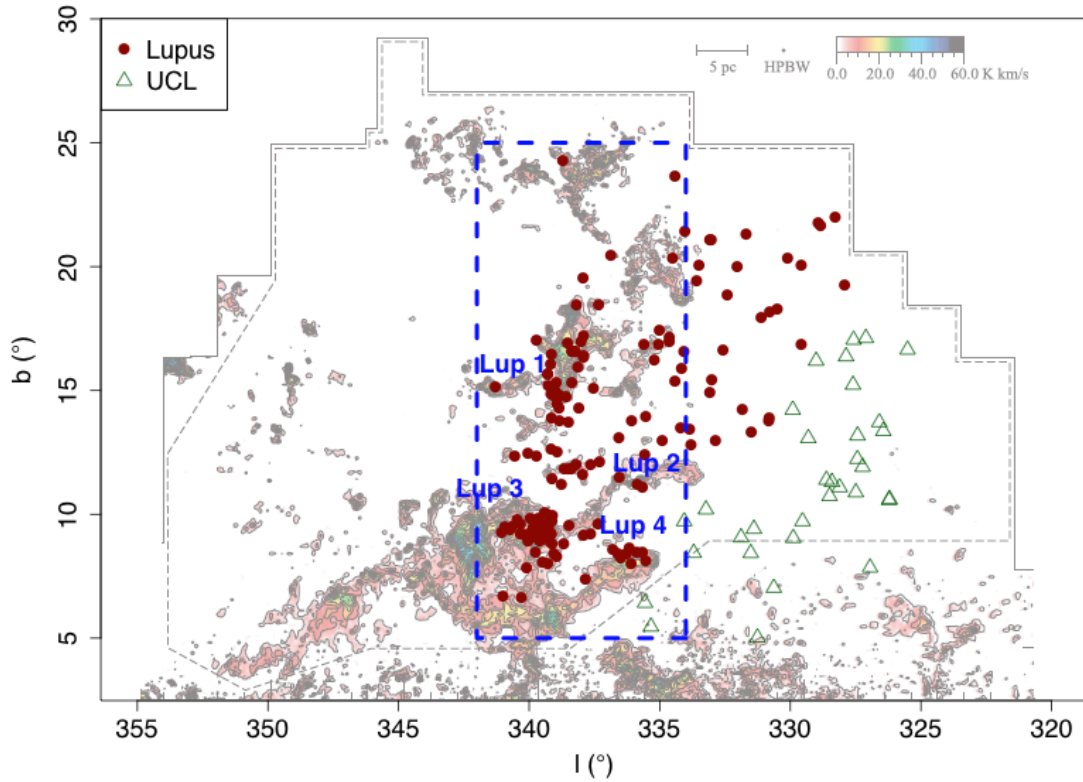


Fig. 6. Location of the 217 PMS stars overlaid on the ^{12}CO intensity map of Tachihara et al. (2001). Different symbols and colors indicate the membership classification (Lupus or UCL) that results from our k-NN analysis.

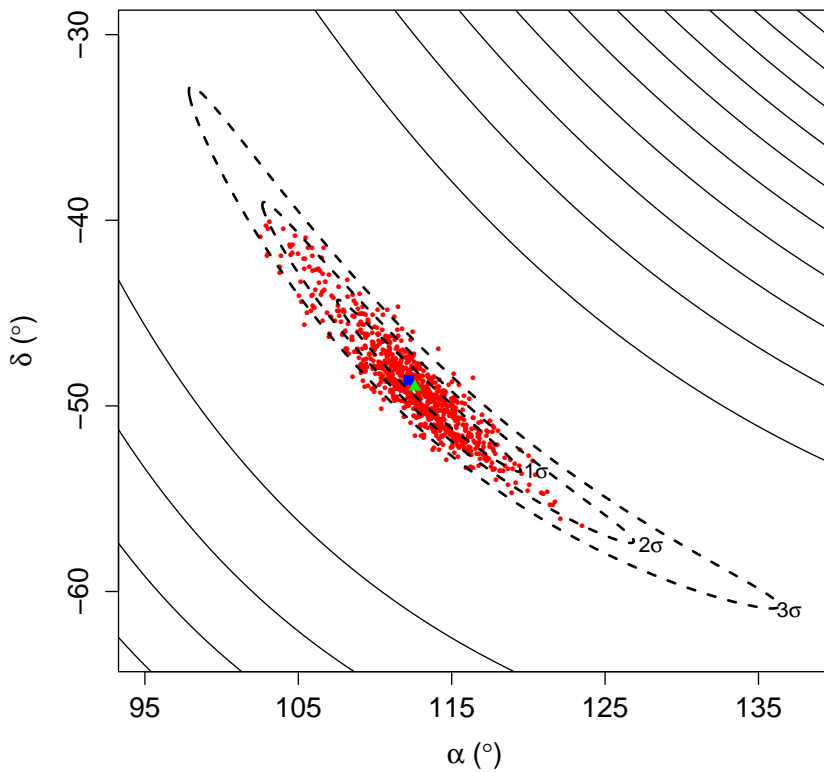


Fig. 7. Realizations of CP coordinates for 1000 Monte Carlo simulations (red dots) overlaid on the X^2 contours (solid lines) for the CP solution derived in Sect. 5.3. The blue square denotes the CP coordinates for the Lupus moving group derived in that section, and the green triangle denotes the centroid distribution of simulated CPs (see Sect. 5.4). The dashed lines indicate the 1σ , 2σ , and 3σ contour levels of our CP solution.

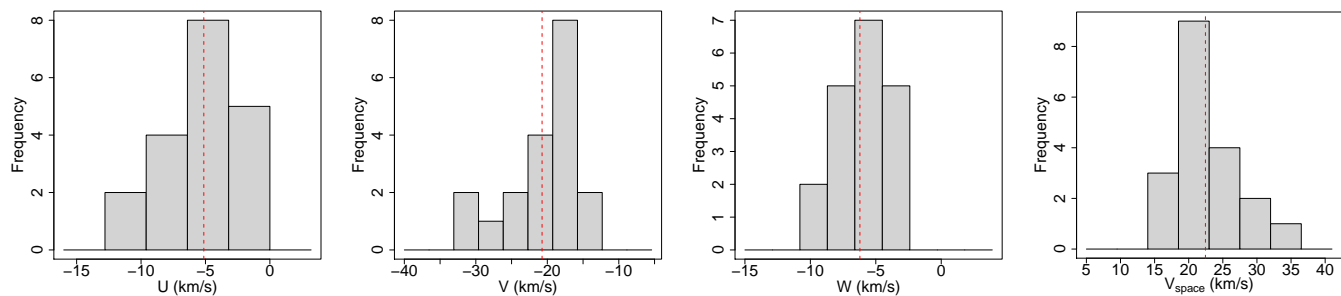


Fig. 8. Histograms of the Galactic velocity components for members of the Lupus moving group with known RVs. The red dashed line denotes the average values given in Sect. 6.1.

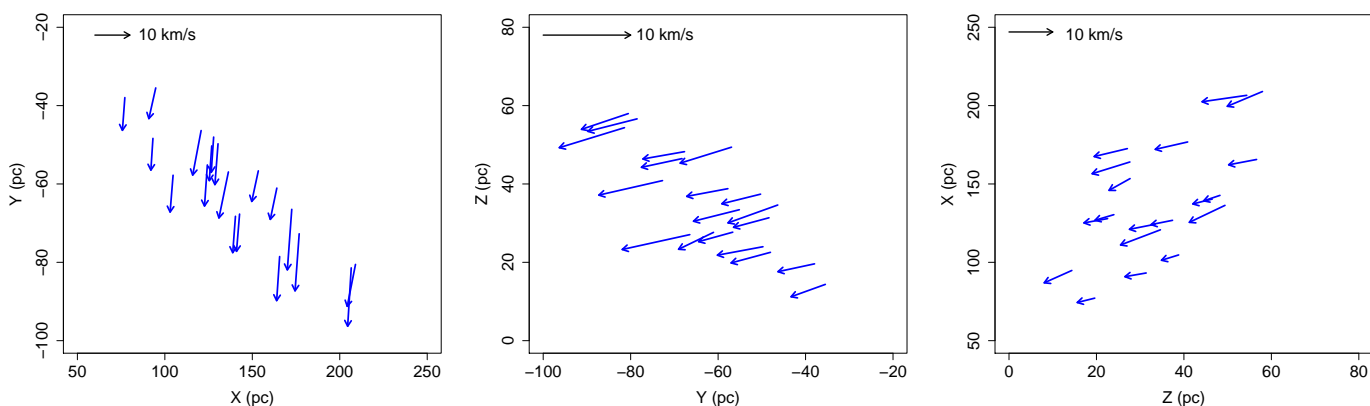


Fig. 9. Spatial velocities of the 19 group members of the Lupus moving group with known RVs projected on the XY , YZ and ZX planes.

Table 5. Proper motion and RV for the 19 stars that define the Lupus core moving group.

Star	α (h:m:s)	δ ($^{\circ}$ ' '')	$\mu_{\alpha} \cos \delta$ (mas/yr)	μ_{δ} (mas/yr)	Source	V_r (km/s)	Ref.	2MASSJ
RXJ1508.8-3715	15 08 53.8	-37 15 46	-20.8 ± 1.3	-24.1 ± 1.2	SPM4	$+4.5 \pm 0.3$	1	15085379-3715467
RXJ1518.4-3738*	15 18 26.9	-37 38 02	-18.1 ± 1.3	-26.5 ± 1.2	SPM4	$+3.7 \pm 0.4$	2	15182692-3738021
RXJ1524.5-3652	15 24 32.4	-36 52 02	-14.8 ± 2.7	-19.6 ± 2.8	SPM4	$+3.8 \pm 0.3$	1	15243236-3652027
RXJ1525.0-3604	15 25 03.6	-36 04 45	-14.4 ± 2.3	-21.1 ± 2.5	SPM4	$+4.3 \pm 0.5$	3	15250358-3604455
RXJ1525.5-3613	15 25 33.2	-36 13 46	-15.7 ± 2.1	-19.1 ± 2.2	SPM4	$+3.6 \pm 0.1$	4	15253316-3613467
RXJ1531.3-3329	15 31 22.0	-33 29 39	-21.7 ± 1.7	-29.2 ± 1.8	SPM4	-3.6 ± 0.5	5	15312193-3329394
RXJ1534.6-4003K	15 34 38.2	-40 02 27	-24.0 ± 1.4	-32.8 ± 1.4	SPM4	$+3.8 \pm 0.9$	6	15343816-4002280
RXJ1540.7-3756	15 40 41.2	-37 56 18	-17.7 ± 1.1	-27.4 ± 1.1	SPM4	$+3.9 \pm 1.0$	3	15404116-3756185
RXJ1544.5-3521	15 44 35.3	-35 21 49	-14.7 ± 2.4	-23.2 ± 2.4	SPM4	$+2.5 \pm 0.2$	1	15443529-3521492
Sz73	15 47 57.0	-35 14 35	-21.0 ± 13.2	-35.4 ± 16.2	SPM4	-3.3 ± 0.2	7	15475693-3514346
GQLup	15 49 12.1	-35 39 04	-11.8 ± 2.7	-19.0 ± 2.5	SPM4	-3.2 ± 0.7	7	15491210-3539051
RXJ1549.9-3629	15 49 59.2	-36 29 57	-13.7 ± 1.6	-25.6 ± 1.6	SPM4	$+4.4 \pm 1.0$	3	15495920-3629574
RXJ1552.3-3819	15 52 19.5	-38 19 31	-17.6 ± 1.1	-27.2 ± 1.2	SPM4	$+4.9 \pm 1.0$	3	15521952-3819313
RXJ1605.7-3905*	16 05 45.0	-39 06 06	-17.7 ± 2.2	-26.4 ± 2.1	SPM4	$+3.2 \pm 0.9$	6	16054499-3906065
F304	16 08 11.0	-39 10 46	-13.6 ± 2.0	-25.2 ± 2.0	SPM4	$+2.8 \pm 0.1$	1	16081096-3910459
RXJ1608.5-3847	16 08 31.6	-38 47 29	-12.0 ± 2.3	-19.2 ± 2.4	SPM4	-2.5 ± 1.0	3	16083156-3847292
RXJ1610.0-4016	16 10 04.8	-40 16 12	-18.6 ± 2.0	-30.7 ± 2.0	SPM4	$+5.1 \pm 1.0$	3	16100478-4016122
Sz121	16 10 12.2	-39 21 18	-8.3 ± 2.4	-21.6 ± 2.5	SPM4	-2.8 ± 2.0	8	16101219-3921181
RXJ1613.0-4004	16 13 02.4	-40 04 33	-17.2 ± 1.5	-33.9 ± 1.5	SPM4	-2.8 ± 1.0	3	16130240-4004329

Notes. The symbol “*” indicates those stars whose membership status (Lupus or UCL) is doubtful in the literature. We provide for each star the most usual identifier, position (epoch 2000), proper motion, source of proper motion, RV, source of RV, and the 2MASS identifier.

References. Radial velocity sources: (1) This work; (2) James et al. (2006); (3) Wichmann et al. (1999); (4) Guenther et al. (2007); (5) White et al. (2007); (6) Torres et al. (2006); (7) Melo (2003); (8) Dubath et al. (1996).

Table 6. Individual parallax and velocity components for Lupus stars with known RVs.

Star	π (mas)	U (km/s)	V (km/s)	W (km/s)	V_{space} (km/s)
RXJ1508.8-3715	8.0 ± 1.4	-3.4 ± 1.3	-18.8 ± 2.1	-3.9 ± 2.4	19.5 ± 2.1
RXJ1518.4-3738	9.1 ± 1.8	-2.4 ± 1.1	-16.2 ± 2.2	-4.9 ± 2.5	17.1 ± 2.2
RXJ1524.5-3652	6.1 ± 1.4	-3.1 ± 1.7	-18.6 ± 3.4	-4.4 ± 3.7	19.3 ± 3.4
RXJ1525.0-3604	5.2 ± 1.3	-3.4 ± 1.9	-22.5 ± 4.1	-6.4 ± 4.6	23.6 ± 4.1
RXJ1525.5-3613	6.1 ± 1.3	-3.5 ± 1.5	-19.0 ± 3.1	-3.7 ± 3.3	19.7 ± 3.0
RXJ1531.3-3329	6.4 ± 2.0	-10.8 ± 2.4	-23.5 ± 5.5	-8.2 ± 5.9	27.1 ± 5.2
RXJ1534.6-4003K	11.3 ± 3.3	-2.8 ± 1.6	-16.7 ± 3.2	-4.0 ± 3.6	17.4 ± 3.2
RXJ1540.7-3756	7.1 ± 2.3	-3.2 ± 2.0	-21.0 ± 4.6	-5.9 ± 5.1	22.0 ± 4.6
RXJ1544.5-3521	7.1 ± 2.1	-2.7 ± 1.5	-17.7 ± 3.9	-4.9 ± 4.2	18.6 ± 3.9
Sz73	7.5 ± 3.4	-9.7 ± 4.4	-22.7 ± 11.8	-9.1 ± 12.5	26.3 ± 11.2
GQLup	4.3 ± 1.6	-9.4 ± 2.5	-21.4 ± 6.6	-8.0 ± 7.0	24.7 ± 6.2
RXJ1549.9-3629	4.4 ± 1.5	-4.1 ± 2.5	-29.8 ± 7.4	-10.2 ± 8.0	31.8 ± 7.4
RXJ1552.3-3819	5.1 ± 1.5	-4.7 ± 2.4	-29.1 ± 6.1	-7.4 ± 6.6	30.4 ± 6.0
RXJ1605.7-3905	7.1 ± 2.7	-3.6 ± 2.1	-20.8 ± 5.6	-4.3 ± 5.9	21.6 ± 5.5
F304	7.2 ± 1.8	-2.7 ± 1.1	-18.0 ± 3.5	-5.4 ± 3.6	19.0 ± 3.5
RXJ1608.5-3847	6.0 ± 2.9	-7.5 ± 2.2	-15.6 ± 6.1	-4.8 ± 6.4	18.0 ± 5.6
RXJ1610.0-4016	5.4 ± 1.6	-5.1 ± 2.4	-30.9 ± 6.7	-7.6 ± 7.0	32.2 ± 6.6
Sz121	5.6 ± 4.3	-7.5 ± 3.3	-16.0 ± 10.3	-8.6 ± 10.7	19.6 ± 9.7
RXJ1613.0-4004	9.8 ± 4.2	-7.9 ± 1.9	-15.7 ± 5.4	-6.3 ± 5.6	18.6 ± 5.0

Notes. We provide the most usual identifier, individual parallax, and velocity components for each star.

There is therefore no reason to reject those stars with $V_r < 0$ from our analysis. Owing to the negligible impact to our results and for clarity of presentation we have decided not to present the re-evaluated parallaxes and space velocities.

6.2. Approximate parallaxes for other moving group members

The hypothesis that all members of a moving group share the same space motion allows us to compute tentative parallaxes for group members with unknown RVs. First we derive the average spatial velocity V_{space} from the Galactic velocity of the stars with known RVs using the 19 stars that define the Lupus core moving group (see Sect. 6.1). Then we compute an approximate parallax π_{app} as

$$\pi_{app} = \frac{A\mu_{\parallel}}{V_{space} \sin \lambda}. \quad (5)$$

The uncertainty on this tentative parallax is again derived by error propagation and considers in this case the error budget of proper motions, space velocity, and the CP errors. We present in Fig. 10 a comparison between individual parallaxes (see Table 5) and approximate parallaxes for the Lupus core moving group. Both procedures return similar results within the admittedly large error bars, which tends to justify the assumption of a common space motion.

The velocity dispersion of the cluster prevents all stars from having exactly the same space velocity. However, the procedure described above for deriving approximate parallaxes considers a single value of the space velocity for all stars in the group. We performed Monte Carlo simulations by resampling the spatial velocity from a Gaussian distribution where the mean and variance correspond to the values given in Sect. 6.1 for the average space velocity of the Lupus core moving group. We constructed a total of 1000 realizations. In each run we assigned a different

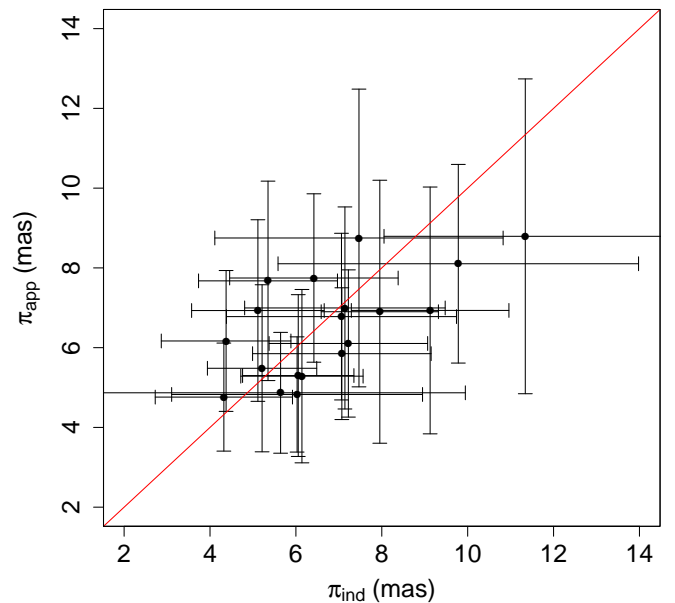


Fig. 10. Comparison of parallaxes computed with RVs (π_{ind}) and the spatial velocity (π_{app}) for the Lupus core moving group of 19 stars. The red solid line indicates perfect correlation. The mean difference between parallaxes computed with both strategies is 0.2 mas, and the rms is 1.4 mas.

value of space velocity and derived the approximate parallax for each star by using Eq. (5). The average value of the computed parallaxes gives our final result, and the standard error of the mean is propagated into the parallax uncertainty. This strategy

not only allows us to reproduce the effect of velocity dispersion, but also makes our parallax results less dependent on a single value used for the spatial velocity of the group. We present in Table 7 the approximate parallaxes derived for the remaining 90 Lupus stars with unknown RVs.

We do stress, however, that the individual approximate parallaxes derived in this way should only be seen as tentative values that will be useful for preliminary statistical analyses of the Lupus association. They should be superseded by more precise values when RV measurements become available for these association members.

6.3. Comparison with Hipparcos parallaxes

As a final check of our results we compare the parallaxes derived in this work with HIPPARCOS trigonometric parallaxes. We consider both versions of the catalog: the original catalog (ESA 1997, hereafter HIP97), and the new reduction of HIPPARCOS data (van Leeuwen 2007, hereafter HIP07). We found only six HIPPARCOS stars among the 109 moving group members and used the group spatial velocity to compute approximate parallaxes. The results of this comparison are presented in Fig. 11. The rms with respect to HIP97 is 2.7 mas and 2.5 mas for HIP07. The mean difference between the parallaxes derived in this work and the ones in HIP97 and HIP07 are -0.9 mas and $+0.8$ mas, respectively. We conclude that our results are in good agreement with the trigonometric parallaxes given in HIPPARCOS.

6.4. Comparison with Makarov (2007) results

Makarov (2007) estimated kinematic distances for Lupus stars in a similar manner to the procedure described in Sect. 6.2. To do so, he assumed a mean spatial velocity of 22 km/s and used the derived distances to infer the depth of the Lupus association. In the following we discuss these findings in light of our own results derived in this study.

The sample of 109 moving group members defined in our CP analysis is cross-correlated with the 93 stars used by Makarov (2007) resulting in 44 stars. When comparing the parallaxes derived in both studies we find a mean difference of $\Delta\pi = -0.9 \pm 0.2$ mas (in the sense “this work” minus “Makarov 2007”) with rms of 1.5 mas (see Fig. 12). In Sect. 6.1 we derived a mean space velocity of $V_{space} = 22.5 \pm 1.1$ km/s that confirms the value of 22 km/s used by Makarov (2007) in his analysis. Since the difference between both values amounts to only 2%, it seems unlikely that the reported systematic effect between the two parallax sets can only be explained by the adopted value of the group spatial velocity. As discussed in Sect. 5.3 the CP position derived in both studies differs significantly by $\Delta\lambda = 25.4^\circ \pm 8.3^\circ$.

It is also important to note that the proper motions used in each work play an important role not only for determining the CP position, but also for deriving the parallaxes of group members. When we use proper motions from the UCAC2 catalog as done by Makarov (2007) with the CP derived in this paper, the mean difference between the parallaxes presented in both studies drops to $\Delta\pi = -0.5 \pm 0.2$ mas. This result is illustrated in Fig. 12. However, given the more recent and precise astrometric catalogs available now, such as the ones used in this paper (see Sect. 3.1), there is no good reason to use the UCAC2 catalog where the proper motions for some stars are poorly defined with only two observational data points. That Table 2 of Makarov (2007) does not include the uncertainty of the computed distances makes it difficult to compare the quality of both

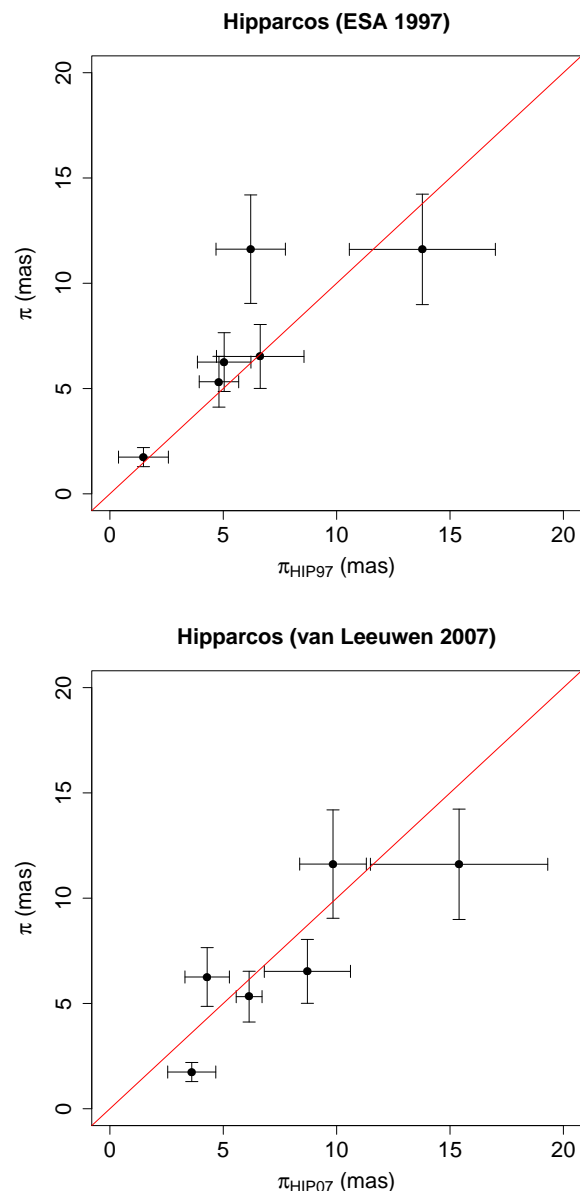


Fig. 11. Parallaxes derived in this paper compared with the trigonometric parallaxes given in HIP97 (*upper panel*) and HIP07 (*lower panel*). The red solid line represents the expected distribution for equal results.

parallax results. The average error of the proper motions used in this paper and by Makarov (2007) is, respectively, 1.9 mas/yr and 3.3 mas/yr in each component. Given the proper motion and CP errors (see Sects. 5.1 and 5.3) presented in both studies we conclude that the parallaxes derived in this paper are more precise and accurate, because our results take the various sources of errors included in the parallax computation into account.

To investigate the depth of the Lupus moving group we first determine the so-assumed center of the association, $(X_C, Y_C, Z_C) = (142, -61, 38)$ pc, as defined by the 19 stars in Table 5, and then compute the distance of all 109 group members to the center of the association. Figure 13 displays the histogram of the computed distances. We conclude that the Lupus association shows a large depth of at least 100 pc, exceeding the value of 80 pc reported by Makarov (2007). However, we stress that a more detailed study about the spatial distribution of Lupus

stars and the size of the association is necessary when more RVs become available in the future.

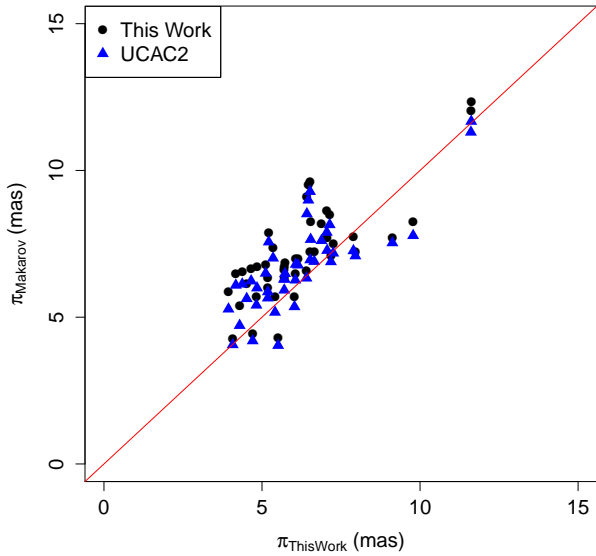


Fig. 12. Comparison between the parallaxes derived in this work and by Makarov (2007). Parallaxes are calculated using the proper motion catalogs included in this work (see Sect. 3.1) and UCAC2 following Makarov (2007). The red solid line indicates perfect correlation.

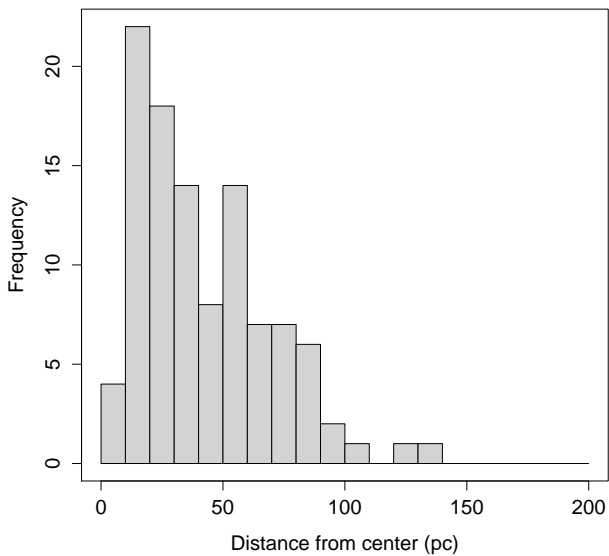


Fig. 13. Histogram of the individual distances of the 109 Lupus moving group members to the center of the association.

7. Discussion

7.1. Positions and parallaxes for pre-main sequence subclasses

The Lupus moving group identified in this paper contains 39 CTTs, 68 WTTs, and 2 HAeBes. Among the WTTs we have 49 on-cloud and 19 off-cloud stars. Figure 14 displays the location of the various PMS subclasses. We note that the Lupus 4 population consists mainly of CTTs, while in the remaining clouds we find both CTTs and WTTs, which may represent a selection effect of our input list of Lupus candidate stars (see Sect. 3). As already predicted, the off-cloud population contains only WTTs while the CTTs are located in the immediate vicinity of the molecular clouds.

An interesting point arises when we compare the distances of these various TTS populations. Indeed, we find that the off-cloud WTTs tend to be closer to us and the CTTs more distant. We present in Table 8 the average parallaxes (distances) for each subgroup in the Lupus SFR.

Table 8. Properties of the TTSs in Lupus.

Sample	Stars	π (mas)	d (pc)
CTTS	39	4.8 ± 0.2	208^{+9}_{-8}
WTTs (on-cloud)	49	6.0 ± 0.3	167^{+9}_{-8}
WTTs (off-cloud)	19	7.2 ± 0.5	139^{+10}_{-9}

Notes. For each TTS subclass we provide the number of stars, average parallax and average distance with the corresponding uncertainties.

7.2. Notes on the parallaxes of Lupus subgroups

The parallaxes derived in this paper allow us to investigate the properties of the various subgroups in this cloud complex. Figure 15 displays the location of Lupus members and corresponding clouds. The histogram of parallaxes is presented in Fig. 16. In the following we discuss the parallaxes derived for these subgroups based on the results presented in Table 9. Using the information provided in Table 2 we calculate the mean UVW velocities for each subgroup and confirm that they exhibit coherent motions with a one-dimensional velocity dispersion of ~ 1 km/s among the various subgroups (see Table 9).

Table 9. Properties of the various subgroups in Lupus.

Sample	Stars	π (mas)	d (pc)	(U, V, W) (km/s)
Lupus 1	21	5.5 ± 0.2	182^{+7}_{-6}	(-4,-21,-5)
Lupus 2	12	6.0 ± 0.6	167^{+19}_{-15}	(-5,-21,-5)
Lupus 3	50	5.4 ± 0.3	185^{+11}_{-10}	(-5,-19,-6)
Lupus 4	7	4.9 ± 0.4	204^{+18}_{-15}	(-7,-20,-9)
Lupus (off-cloud)	19	7.2 ± 0.5	139^{+10}_{-9}	(-4,-19,-4)
Lupus (full sample)	109	5.8 ± 0.2	172^{+6}_{-6}	(-5,-20,-6)

Notes. We provide for each subgroup the number of stars, average parallax, and average distance with the corresponding uncertainties and the mean UVW velocity components. Uncertainties in the mean velocities are 1-2 km/s. Those stars in the on-cloud region (see definition in Sect. 3.2) located beyond the limits of the main molecular clouds (Lupus 1-4) have been assigned to the off-cloud population (see Fig. 15).

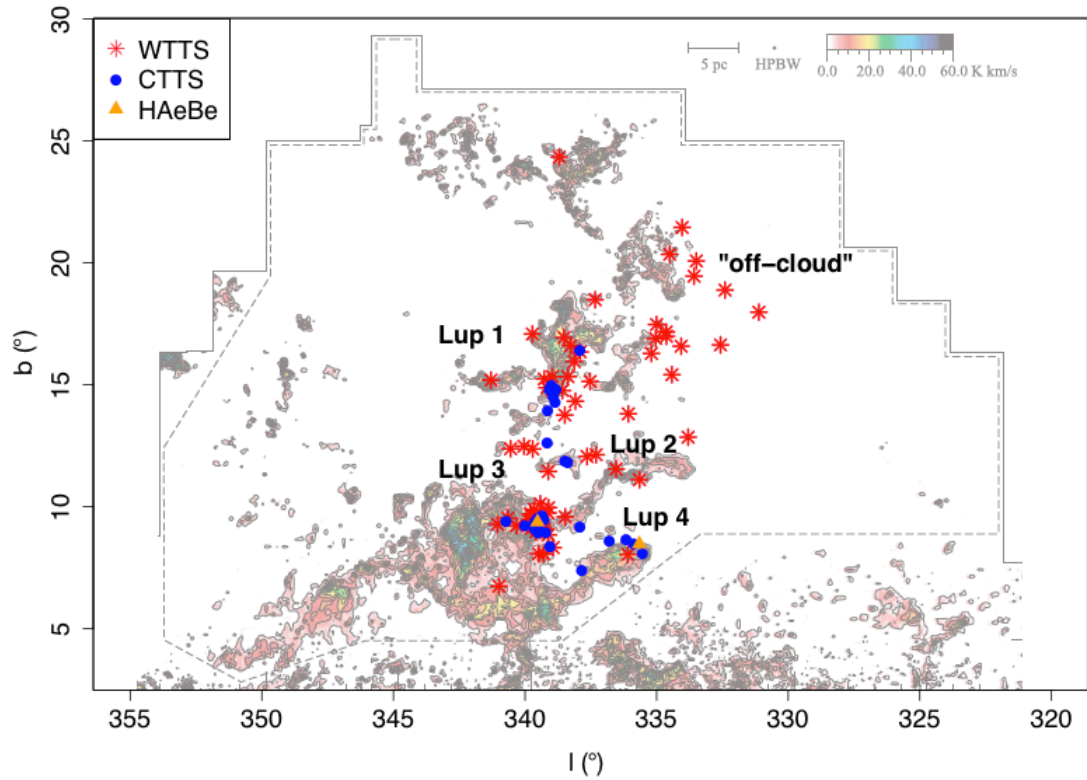


Fig. 14. Location of the moving group members overlaid on the ^{12}CO intensity map from Tachihara et al. (2001). Different symbols and colors mark the various YSO subclasses.

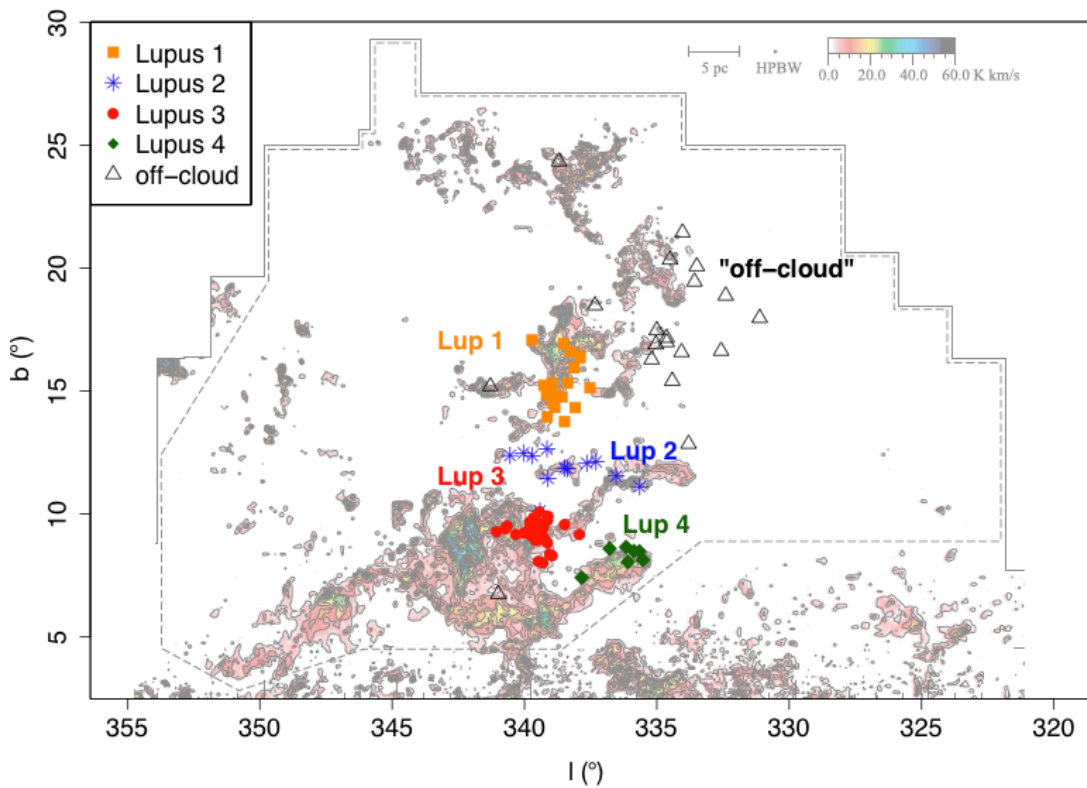


Fig. 15. Location of the moving group members overlaid on the ^{12}CO intensity map from Tachihara et al. (2001). Different symbols and colors mark the various clouds of the Lupus complex.

Full sample: The average error on parallaxes is $\bar{\sigma}_\pi = 1.5$ mas, yielding an average precision of about 25% in our distance results derived in this paper. We note the existence of background and foreground populations (as anticipated in Sect. 3), confirming that the Lupus complex occupies a large volume in space.

Off-cloud population: The WTTs that form this population are scattered not only in angular extent but also in depth (see Fig. 16). Different scenarios have been suggested to explain the dispersed population of WTTs: the stars may have been formed in the vicinity of the clouds and have reached their present location because of the velocity dispersion in the group (Wichmann et al. 1997a); they might have been ejected with high velocities by dynamical interactions in multiple systems (Sterzik & Durisen 1995); star formation could have occurred in small cloudlets that have now dispersed (Feigelson 1996). One important parameter in this discussion is the stellar age that can now be accurately determined for those stars with individual parallaxes. Age determination goes beyond the scope of the present work and will be discussed in a forthcoming paper.

Lupus 1, 2, and 4: All together they contain 37% of moving group members. While Lupus 1 and 2 are somewhat closer, Lupus 4 is more distant (see Table 9). We derived individual parallaxes for four stars in Lupus 1 and one star in Lupus 2. Our results for Lupus 4 are less accurate, because we only computed tentative parallaxes, and our sample is biased towards CTTSs as mentioned before. However, Hip 78092 is an HAeBe star projected in the direction of Lupus 4, and HIPPARCOS results for this star, $\pi_{HIP97} = 5.04 \pm 1.18$ mas and $\pi_{HIP07} = 4.29 \pm 0.98$ mas, confirm the approximate distance to the cloud derived in this paper.

Lupus 3: We find significant depth effects in Lupus 3, while the stars in the remaining clouds are less dispersed along the line of sight (see, e.g., Fig. 16). One possibility for explaining this result is the existence of various components along the line of sight that lie at different distances. We computed the average parallax of the CTTSs (26 stars) and WTTs (23 stars) in Lupus 3 and find

$$\bar{\pi}_{CTTS} = 4.6 \pm 0.2 \text{ mas},$$

$$\bar{\pi}_{WTTs} = 6.1 \pm 0.4 \text{ mas}.$$

The depth of Lupus 3 derived from the closest and remotest parts of this cloud is in good agreement with Lombardi et al. (2008, see Sect. 2). This preliminary result must be confirmed by further investigations since we derived accurate parallaxes for only a few stars.

7.3. Expansion of the Lupus association

In Sect. 6.1 we mentioned that the Lupus association is undergoing expansion (see also Makarov 2007). From the proper motions alone, it is impossible to distinguish between the state of linear expansion and parallel space motions, so RVs are needed to distinguish between them. In the following we use the Blaauw's expansion model (Blaauw 1964), combined with the radial velocities and individual parallaxes given in Tables 5 and 6, to investigate whether the expansion rate of the association can be detected.

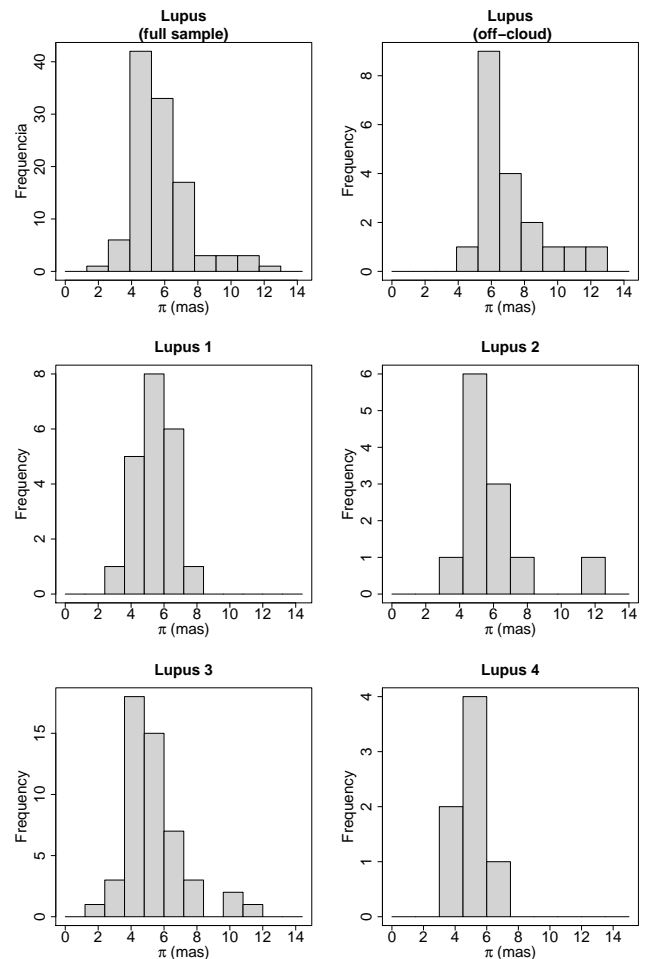


Fig. 16. Histogram of parallaxes for the various subgroups of the Lupus complex.

In the Blaauw model for linear expansion the stellar RVs are given by

$$V_r = V_{space} \cos \lambda + \kappa d + K, \quad (6)$$

where κ is the expansion term, K a systematic error in the radial velocities, and d the individual distance of the star. A linear expansion exists when $\kappa > 0$ in this equation. To derive κ , we plot the difference between the observed spectroscopic RVs and the predicted RVs ($V_r^{pred} = V_{space} \cos \lambda$) inferred from the CP coordinates as a function of the individual distances. Then, we solve for the slope κ in Eq. 6 (see Figure 17). The best fit to the data yields $\kappa = 0.021 \pm 0.004 \text{ km s}^{-1} \text{ pc}^{-1}$. We reject GQ Lup, RXJ1608.5-3847, and Sz121 from this analysis, because of the large errors in distance (see Table 6), and RXJ1613.0-4004 because of its large deviation, presumably due to a poor RV. Although the derived expansion term κ is small when compared to, say, the TW Hydrae association (see Mamajek 2005), it is positive within 3σ of the computed uncertainty. This result confirms that the linear expansion in the Lupus association of young stars is real but small.

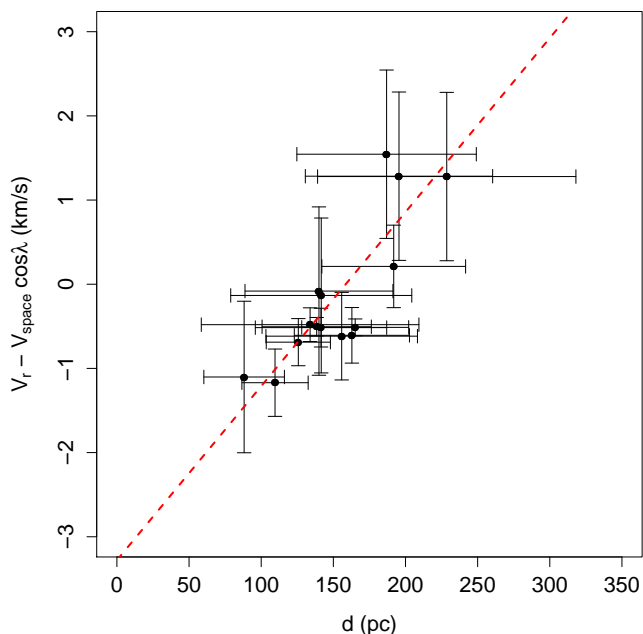


Fig. 17. Blaauw’s linear expansion model applied to the Lupus association of young stars. The red dashed line indicates the weighted least-squares fit to the data.

8. Conclusions

We have identified a moving group of 109 stars in the Lupus SFR by applying our new CP search method combined with the k-NN algorithm, which made it possible to perform a membership analysis and to distinguish between Lupus and UCL stars. We applied the CP search method to different subsets of association members and confirmed our solution with Monte Carlo simulations. Because of the close proximity to the UCL subgroup and the difficulties encountered in separating these groups, we claim that we have detected a *minimum* moving group in our CP analysis that may not contain all stars kinematically associated to Lupus. We derived accurate parallaxes for members with known RVs that we define as the Lupus core moving group and used the group spatial velocity to tentatively calculate approximate parallaxes for the remaining stars.

Determination of individual parallaxes is restricted to moving group members with known RVs. The RVs of many stars in the group either have never been measured or are of low quality so cannot be used to derive accurate parallaxes. We presented new RV measurements for 52 PMS stars of our starting sample of Lupus candidate stars based on spectroscopic observations performed with FEROS. We encourage observers to employ the available precise spectrographs to perform spectroscopic surveys of this complex SFR. Additional observations will also allow one to detect new binaries and confirm the youth of many PMS candidates.

We show that the CTTs are located close to or within the molecular clouds, while the WTTs are dispersed not only in angular extent but also in depth. We find evidence of depth effects in Lupus 3 that must be confirmed by further investigations. Based on the individual distances and radial velocities derived in this paper, we also confirm that the Lupus association is undergoing expansion. These results represent a first step toward better understanding of the structure of the Lupus cloud com-

plex. The individual distances derived in this paper will be used in a forthcoming paper to investigate the physical properties of Lupus stars.

Acknowledgements. It is a pleasure to thank Johnny Setiawan and Maren Mohler for their assistance with the FEROS Data Reduction Software and cross-correlation techniques used for radial velocity computations. We thank Kengo Tachihara for providing the image for Figures 3, 6, 14, and 15, and the PASJ editorial office for granting permission to reproduce this material. We also acknowledge the referee for the careful report. This research was funded by a doctoral/post-doctoral fellowship from FAPESP and made use of the SIMBAD database operated at the CDS, Strasbourg, France.

References

- Appenzeller, I. & Mundt, R. 1989, *A&A Rev.*, 1, 291
 Ball, N. M., Brunner, R. J., Myers, A. D., et al. 2007, *ApJ*, 663, 774
 Baranne, A., Queloz, D., Mayor, M., et al. 1996, *A&AS*, 119, 373
 Barbier-Brossat, M. & Figon, P. 2000, *A&AS*, 142, 217
 Barbier-Brossat, M., Petit, M., & Figon, P. 1994, *A&AS*, 108, 603
 Basri, G., Martin, E. L., & Bertout, C. 1991, *A&A*, 252, 625
 Bertout, C. 1987, in *IAU Symposium*, Vol. 122, *Circumstellar Matter*, ed. I. Appenzeller & C. Jordan, 23–38
 Bertout, C., Basri, G., & Bouvier, J. 1988, *ApJ*, 330, 350
 Bertout, C. & Genova, F. 2006, *A&A*, 460, 499
 Bertout, C., Robichon, N., & Arenou, F. 1999, *A&A*, 352, 574
 Blaauw, A. 1964, *ARA&A*, 2, 213
 Bobylev, V. V. 2006, *Astronomy Letters*, 32, 816
 Chen, C. H., Mamajek, E. E., Bitner, M. A., et al. 2011, *ApJ*, 738, 122
 Comerón, F. 2008, *The Lupus Clouds*, ed. Reipurth, B., 295
 Correia, S., Zinnecker, H., Ratzka, T., & Sterzik, M. F. 2006, *A&A*, 459, 909
 de Bruijne, J. H. J. 1999, *MNRAS*, 310, 585
 de Zeeuw, P. T., Hoogerwerf, R., de Bruijne, J. H. J., Brown, A. G. A., & Blaauw, A. 1999, *AJ*, 117, 354
 Dubath, P., Reipurth, B., & Mayor, M. 1996, *A&A*, 308, 107
 Ducourant, C., Teixeira, R., Périé, J. P., et al. 2005, *A&A*, 438, 769
 Duflot, M., Figon, P., & Meyssonnier, N. 1995, *A&AS*, 114, 269
 Dzib, S., Loinard, L., Mioduszewski, A. J., et al. 2010, *ApJ*, 718, 610
 Dzib, S., Loinard, L., Rodríguez, L. F., Mioduszewski, A. J., & Torres, R. M. 2011, *ApJ*, 733, 71
 ESA. 1997, *VizieR Online Data Catalog*, 1239, 0
 Feigelson, E. D. 1996, *ApJ*, 468, 306
 Fix, E. & Hodges, J. 1951, *Discriminatory analysis. Nonparametric discrimination: Consistency properties*, Technical Report 4, Project Number 21-49-004, USAF School of Aviation Medicine, Randolph Field, Texas
 Galli, P. A. B., Teixeira, R., Ducourant, C., Bertout, C., & Benevides-Soares, P. 2012, *A&A*, 538, A23
 Ghez, A. M., McCarthy, D. W., Patience, J. L., & Beck, T. L. 1997, *ApJ*, 481, 378
 Girard, T. M., van Altena, W. F., Zacharias, N., et al. 2011, *AJ*, 142, 15
 Gontcharov, G. A. 2006, *Astronomy Letters*, 32, 759
 Gregorio-Hetem, J., Lepine, J. R. D., Quast, G. R., Torres, C. A. O., & de La Reza, R. 1992, *AJ*, 103, 549
 Grenier, S., Burnage, R., Faraggiana, R., et al. 1999, *A&AS*, 135, 503
 Guenther, E. W., Esposito, M., Mundt, R., et al. 2007, *A&A*, 467, 1147
 Herbig, G. H. 1962, *Advances in Astronomy and Astrophysics*, 1, 47
 Herbig, G. H. & Bell, K. R. 1988, *Third Catalog of Emission-Line Stars of the Orion Population : 3 : 1988*, ed. Herbig, G. H. & Bell, K. R.
 Høg, E., Fabricius, C., Makarov, V. V., et al. 2000, *A&A*, 355, L27
 Hughes, J., Hartigan, P., & Clampitt, L. 1993, *AJ*, 105, 571
 James, D. J., Melo, C., Santos, N. C., & Bouvier, J. 2006, *A&A*, 446, 971
 Johnson, D. R. H. & Soderblom, D. R. 1987, *AJ*, 93, 864
 Jones, B. F. & Herbig, G. H. 1979, *AJ*, 84, 1872
 Joy, A. H. 1945, *ApJ*, 102, 168
 Kaufer, A., Stahl, O., Tubbesing, S., et al. 1999, *The Messenger*, 95, 8
 Kharchenko, N. V., Scholz, R.-D., Piskunov, A. E., Röser, S., & Schilbach, E. 2007, *Astronomische Nachrichten*, 328, 889
 Knude, J. & Hog, E. 1998, *A&A*, 338, 897
 Knude, J. & Nielsen, A. S. 2001, *A&A*, 373, 714
 Krautter, J., Wichmann, R., Schmitt, J. H. M. M., et al. 1997, *A&AS*, 123, 329
 Loinard, L., Torres, R. M., Mioduszewski, A. J., et al. 2007, *ApJ*, 671, 546
 Lombardi, M., Lada, C. J., & Alves, J. 2008, *A&A*, 480, 785
 López Martí, B., Jiménez-Esteban, F., & Solano, E. 2011, *A&A*, 529, A108
 Luhman, K. L., Mamajek, E. E., Allen, P. R., & Cruz, K. L. 2009, *ApJ*, 703, 399
 Madsen, S., Dravins, D., & Lindegren, L. 2002, *A&A*, 381, 446
 Makarov, V. V. 2007, *ApJ*, 658, 480
 Malaroda, S., Levato, H., & Galliani, S. 2006, *VizieR Online Data Catalog*, 3249
 Mamajek, E. E. 2005, *ApJ*, 634, 1385

- Mamajek, E. E. 2008, *Astronomische Nachrichten*, 329, 10
- Mamajek, E. E., Meyer, M. R., & Liebert, J. 2002, *AJ*, 124, 1670
- Marengo, M. & Sanchez, M. C. 2009, *AJ*, 138, 63
- Mathieu, R. D. 1986, *Highlights of Astronomy*, 7, 481
- Melo, C. H. F. 2003, *A&A*, 410, 269
- Merín, B., Jørgensen, J., Spezzi, L., et al. 2008, *ApJS*, 177, 551
- Nordström, B., Mayor, M., Andersen, J., et al. 2004, *A&A*, 418, 989
- Preibisch, T. & Mamajek, E. 2008, *The Nearest OB Association: Scorpius-Centaurus (Sco OB2)*, ed. Reipurth, B., 235
- Racine, R. 1968, *AJ*, 73, 233
- Reipurth, B., Pedrosa, A., & Lago, M. T. V. T. 1996, *A&AS*, 120, 229
- Roeser, S., Demleitner, M., & Schilbach, E. 2010, *AJ*, 139, 2440
- Schwartz, R. D. 1977, *ApJS*, 35, 161
- Setiawan, J., Pasquini, L., da Silva, L., von der Lühe, O., & Hatzes, A. 2003, *A&A*, 397, 1151
- Sterzik, M. F. & Durisen, R. H. 1995, *A&A*, 304, L9
- Tachihara, K., Toyoda, S., Onishi, T., et al. 2001, *PASJ*, 53, 1081
- Torres, C. A. O., Quast, G. R., da Silva, L., et al. 2006, *A&A*, 460, 695
- Torres, R. M., Loinard, L., Mioduszewski, A. J., et al. 2012, *ApJ*, 747, 18
- Torres, R. M., Loinard, L., Mioduszewski, A. J., & Rodríguez, L. F. 2007, *ApJ*, 671, 1813
- Torres, R. M., Loinard, L., Mioduszewski, A. J., & Rodríguez, L. F. 2009, *ApJ*, 698, 242
- Udry, S., Mayor, M., & Queloz, D. 1999, in *Astronomical Society of the Pacific Conference Series*, Vol. 185, IAU Colloq. 170: Precise Stellar Radial Velocities, ed. J. B. Hearnshaw & C. D. Scarfe, 367
- van Leeuwen, F. 2007, *A&A*, 474, 653
- Venables, W. N. & Ripley, B. D. 2002, *Modern Applied Statistics with S*. Fourth Edition (Springer), ISBN 0-387-95457-0
- Walter, F. M. 1986, *ApJ*, 306, 573
- Weise, P. 2010, PhD thesis, University of Heidelberg
- Weise, P., Launhardt, R., Setiawan, J., & Henning, T. 2010, *A&A*, 517, A88
- White, R. J., Gabor, J. M., & Hillenbrand, L. A. 2007, *AJ*, 133, 2524
- Wichmann, R., Covino, E., Alcalá, J. M., et al. 1999, *MNRAS*, 307, 909
- Wichmann, R., Krautter, J., Covino, E., et al. 1997a, *A&A*, 320, 185
- Wichmann, R., Sterzik, M., Krautter, J., Metanomski, A., & Voges, W. 1997b, *A&A*, 326, 211
- Zacharias, N., Finch, C. T., Girard, T. M., et al. 2012, *VizieR Online Data Catalog*, 1322, 0
- Zacharias, N., Urban, S. E., Zacharias, M. I., et al. 2004, *AJ*, 127, 3043

Table 7. Approximate parallax derived in this paper for Lupus stars with unknown RVs.

Star	α (h:m:s)	δ ($^{\circ}$ ' ")	$\mu_{\alpha} \cos \delta$ (mas/yr)	μ_{δ} (mas/yr)	Source	π (mas)	2MASSJ
RXJ1511.0-3252AB	15 11 04.6	-32 51 30	-14.0 \pm 3.0	-24.0 \pm 3.0	D05	5.9 \pm 1.5	15110450-3251304
RXJ1511.6-3550	15 11 37.0	-35 50 42	-17.9 \pm 1.6	-21.7 \pm 1.6	SPM4	6.1 \pm 1.4	15113696-3550417
RXJ1512.6-3417	15 12 39.8	-34 16 59	-15.6 \pm 1.8	-18.3 \pm 1.7	SPM4	5.2 \pm 1.2	15123981-3416591
HD135127	15 14 39.6	-34 45 41	-17.3 \pm 1.3	-24.3 \pm 1.3	TYCHO2	6.4 \pm 1.4	15143959-3445412
RXJ1515.7-3332K	15 15 45.4	-33 31 59	-23.1 \pm 1.6	-26.4 \pm 1.6	SPM4	7.5 \pm 1.7	15154537-3331597
GSC6770-655	15 19 53.0	-28 02 26	-36.0 \pm 3.0	-45.0 \pm 3.0	D05	12.2 \pm 2.8	15195295-2802266
RXJ1525.6-3537	15 25 36.7	-35 37 32	-21.0 \pm 2.2	-23.1 \pm 2.3	SPM4	6.7 \pm 1.5	15253666-3537319
RXJ1527.3-3603	15 27 22.9	-36 04 09	-23.6 \pm 2.3	-34.4 \pm 2.4	SPM4	8.9 \pm 2.0	15272286-3604087
RXJ1529.3-3737	15 29 19.0	-37 37 20	-19.2 \pm 0.9	-23.5 \pm 0.9	SPM4	6.5 \pm 1.4	15291901-3737205
RXJ1529.7-3628	15 29 47.3	-36 28 37	-16.6 \pm 1.6	-20.8 \pm 1.7	SPM4	5.7 \pm 1.3	15294727-3628374
Sz65	15 39 27.8	-34 46 17	-9.9 \pm 2.9	-21.5 \pm 2.8	SPM4	5.0 \pm 1.3	15392776-3446171
RXJ1539.7-3450	15 39 46.4	-34 51 02	-14.9 \pm 2.0	-19.3 \pm 2.1	SPM4	5.2 \pm 1.2	15394637-3451027
SSTc2dJ154013.7-340142	15 40 13.7	-34 01 43	-4.5 \pm 3.3	-14.0 \pm 3.1	SPM4	3.0 \pm 1.0	15401371-3401429
RXJ1540.3-3426A	15 40 18.5	-34 26 15	-14.7 \pm 3.7	-19.5 \pm 3.6	SPM4	5.2 \pm 1.4	15401850-3426146
SSTc2dJ154148.3-350145	15 41 48.3	-35 01 46	-13.0 \pm 4.1	-17.2 \pm 4.0	SPM4	4.6 \pm 1.3	15414827-3501458
RXJ1542.0-3601	15 42 05.2	-36 01 32	-19.5 \pm 2.3	-23.4 \pm 2.3	SPM4	6.5 \pm 1.5	15420518-3601317
RXJ1544.0-3311*	15 44 03.8	-33 11 11	-18.1 \pm 1.3	-26.9 \pm 1.4	SPM4	6.9 \pm 1.5	15440376-3311110
RXJ1546.6-3618	15 46 41.2	-36 18 47	-12.7 \pm 1.9	-23.8 \pm 2.0	SPM4	5.7 \pm 1.3	15464121-3618472
RXJ1546.7-3459	15 46 45.1	-34 59 47	-17.4 \pm 3.6	-20.6 \pm 3.4	SPM4	5.7 \pm 1.5	15464506-3459473
RXJ1547.1-3540	15 47 08.4	-35 40 19	-13.3 \pm 2.2	-25.7 \pm 2.2	SPM4	6.1 \pm 1.4	15470841-3540195
RXJ1547.6-4018	15 47 41.8	-40 18 26	-18.7 \pm 1.1	-27.6 \pm 1.1	SPM4	7.2 \pm 1.6	15474176-4018267
HMLup	15 47 50.6	-35 28 35	-9.7 \pm 4.1	-22.0 \pm 3.9	SPM4	5.0 \pm 1.4	15475062-3528353
HNLup	15 48 05.2	-35 15 53	-10.3 \pm 7.2	-19.6 \pm 7.1	SPM4	4.7 \pm 1.8	15480523-3515526
RXJ1548.1-3452	15 48 08.9	-34 52 53	-17.9 \pm 2.2	-22.1 \pm 2.1	SPM4	6.0 \pm 1.4	15480893-3452531
RXJ1548.7-3520	15 48 42.5	-35 20 07	-11.2 \pm 2.9	-16.1 \pm 2.8	SPM4	4.2 \pm 1.1	15484253-3520066
RXJ1548.9-3513	15 48 54.1	-35 13 18	-17.4 \pm 2.1	-27.7 \pm 2.1	SPM4	7.0 \pm 1.6	15485411-3513186
Sz76	15 49 30.7	-35 49 51	-16.1 \pm 2.8	-20.8 \pm 2.7	SPM4	5.6 \pm 1.4	15493074-3549514
HD141277*	15 49 45.0	-39 25 09	-18.2 \pm 2.3	-24.4 \pm 2.2	TYCHO2	6.5 \pm 1.5	15494499-3925089
RXJ1550.7-3828	15 50 46.7	-38 29 27	-10.3 \pm 1.3	-16.0 \pm 1.3	SPM4	4.1 \pm 0.9	15504672-3829267
Sz77	15 51 47.0	-35 56 43	-12.5 \pm 2.2	-20.5 \pm 2.1	SPM4	5.1 \pm 1.2	15514695-3556440
RXJ1555.4-3338	15 55 26.3	-33 38 22	-17.8 \pm 1.8	-28.1 \pm 1.8	SPM4	7.0 \pm 1.6	15552621-3338232
Sz81	15 55 50.3	-38 01 33	-15.8 \pm 1.4	-22.4 \pm 1.5	SPM4	5.8 \pm 1.3	15555030-3801329
RXJ1556.0-3655	15 56 02.1	-36 55 28	-9.3 \pm 2.5	-19.2 \pm 2.4	SPM4	4.5 \pm 1.1	15560210-3655282
Sz82	15 56 09.2	-37 56 06	-12.7 \pm 3.9	-21.5 \pm 4.0	SPM4	5.3 \pm 1.4	15560921-3756057
Hip78092	15 56 41.9	-42 19 23	-13.9 \pm 1.0	-25.5 \pm 1.0	TYCHO2	6.3 \pm 1.4	15564188-4219232
Sz126	15 57 24.0	-42 40 04	-13.1 \pm 1.9	-22.3 \pm 2.1	SPM4	5.6 \pm 1.3	15572401-4240044
Sz127	15 57 30.4	-42 10 32	-10.0 \pm 1.7	-12.3 \pm 1.8	SPM4	3.4 \pm 0.8	15573035-4210324
Sz128	15 58 07.3	-41 51 48	-12.9 \pm 3.3	-18.0 \pm 3.3	SPM4	4.8 \pm 1.3	15580732-4151479
RXJ1558.9-3646	15 58 59.8	-36 46 20	-11.6 \pm 3.0	-23.1 \pm 2.9	SPM4	5.5 \pm 1.4	15585980-3646206
CD-3610569	15 59 49.5	-36 28 28	-29.4 \pm 2.7	-46.0 \pm 2.8	TYCHO2	11.6 \pm 2.6	15594951-3628279
RXJ1559.9-3750	15 59 54.2	-37 50 47	-11.0 \pm 1.3	-19.8 \pm 1.3	SPM4	4.8 \pm 1.1	15595416-3750469
SSTc2dJ160000.6-422158	16 00 00.6	-42 21 57	-10.4 \pm 2.3	-15.8 \pm 2.5	SPM4	4.1 \pm 1.0	16000060-4221567
Sz131	16 00 49.4	-41 30 04	-8.3 \pm 5.4	-21.2 \pm 5.3	SPM4	4.8 \pm 1.6	16004943-4130038
RXJ1601.9-3613	16 01 59.2	-36 12 55	-18.6 \pm 2.6	-24.7 \pm 2.6	SPM4	6.5 \pm 1.5	16015918-3612555
EXLup	16 03 05.5	-40 18 25	-9.8 \pm 2.3	-18.2 \pm 2.4	SPM4	4.4 \pm 1.1	16030548-4018254
RXJ1603.8-3938*	16 03 52.5	-39 39 01	-17.1 \pm 2.1	-29.3 \pm 2.1	SPM4	7.3 \pm 1.7	16035250-3939013
HD143978	16 04 57.1	-38 57 15	-27.8 \pm 1.2	-46.8 \pm 1.6	TYCHO2	11.6 \pm 2.6	16045707-3857157
RXJ1605.5-3837	16 05 33.3	-38 37 45	-12.4 \pm 2.5	-22.7 \pm 2.5	SPM4	5.5 \pm 1.3	16053329-3837451
HOLup	16 07 00.6	-39 02 19	-10.1 \pm 2.5	-18.1 \pm 2.5	SPM4	4.4 \pm 1.1	16070061-3902194
Sz90	16 07 10.1	-39 11 03	-6.9 \pm 3.3	-21.4 \pm 3.3	SPM4	4.7 \pm 1.2	16071007-3911033
Sz91	16 07 11.6	-39 03 47	-14.5 \pm 2.6	-17.6 \pm 2.6	SPM4	4.8 \pm 1.2	16071159-3903475
RXJ1607.2-3839	16 07 13.7	-38 39 24	-12.9 \pm 2.1	-18.0 \pm 2.2	SPM4	4.7 \pm 1.1	16071370-3839238
Sz95	16 07 52.3	-38 58 06	-8.2 \pm 2.6	-21.7 \pm 2.6	SPM4	4.9 \pm 1.2	16075230-3858059
RXJ1608.0-3857	16 08 00.0	-38 57 51	-13.4 \pm 2.1	-20.3 \pm 2.1	SPM4	5.2 \pm 1.2	16075996-3857510
Sz96	16 08 12.6	-39 08 33	-8.7 \pm 2.2	-20.1 \pm 2.3	SPM4	4.6 \pm 1.1	16081263-3908334
RXJ1608.3-3843	16 08 18.3	-38 44 05	-20.8 \pm 2.8	-30.7 \pm 2.8	SPM4	7.9 \pm 1.8	16081824-3844052
Sz97	16 08 21.8	-39 04 21	-10.3 \pm 2.7	-19.8 \pm 2.7	SPM4	4.8 \pm 1.2	16082180-3904214
Sz99	16 08 24.0	-39 05 49	-14.6 \pm 4.5	-25.1 \pm 4.5	SPM4	6.2 \pm 1.7	16082404-3905494
RXJ1608.4-3840	16 08 25.2	-38 40 56	-13.2 \pm 2.5	-16.6 \pm 2.5	SPM4	4.5 \pm 1.1	16082519-3840558
Sz102	16 08 29.7	-39 03 11	-12.7 \pm 4.3	-19.7 \pm 4.4	SPM4	5.0 \pm 1.4	16082972-3903110
Sz104	16 08 30.8	-39 05 49	-21.3 \pm 6.6	-22.5 \pm 6.6	SPM4	6.5 \pm 2.0	16083081-3905488
V856Sco	16 08 34.3	-39 06 18	-12.5 \pm 1.2	-21.6 \pm 1.6	TYCHO2	5.3 \pm 1.2	16083427-3906181
RXJ1608.6-3922	16 08 36.2	-39 23 02	-10.6 \pm 2.2	-23.2 \pm 2.2	SPM4	5.4 \pm 1.3	16083617-3923024
SSTc2dJ160839.8-392922	16 08 39.7	-39 29 23	-18.0 \pm 3.9	-27.5 \pm 3.9	SPM4	7.0 \pm 1.8	16083974-3929228
Sz107	16 08 41.8	-39 01 37	-6.1 \pm 3.7	-18.6 \pm 3.7	SPM4	4.1 \pm 1.2	16084179-3901370
SSTc2dJ160853.2-391440	16 08 53.2	-39 14 40	-19.9 \pm 5.0	-23.3 \pm 4.9	SPM4	6.4 \pm 1.8	16085324-3914401

Table 7. continued.

Star	α (h:m:s)	δ ($^{\circ}$ ' ")	$\mu_{\alpha} \cos \delta$ (mas/yr)	μ_{δ} (mas/yr)	Source	π (mas)	2MASSJ
RXJ1608.9-3905	16 08 54.3	-39 06 06	-8.4 ± 2.5	-20.4 ± 2.5	SPM4	4.7 ± 1.2	16085427-3906057
RXJ1608.9-3945	16 08 54.3	-39 46 05	-8.2 ± 2.4	-21.5 ± 2.5	SPM4	4.8 ± 1.2	16085429-3946046
Sz111	16 08 54.7	-39 37 43	-8.1 ± 2.3	-18.9 ± 2.3	SPM4	4.4 ± 1.1	16085468-3937431
Sz112	16 08 55.5	-39 02 34	-9.6 ± 2.8	-18.4 ± 2.9	SPM4	4.4 ± 1.1	16085553-3902339
Sz113	16 08 57.8	-39 02 23	-12.5 ± 3.5	-19.8 ± 3.5	SPM4	5.0 ± 1.3	16085780-3902227
V908Sco	16 09 01.9	-39 05 12	-7.7 ± 2.1	-18.4 ± 2.2	SPM4	4.2 ± 1.0	16090185-3905124
SSTc2dJ160904.6-392112	16 09 04.5	-39 21 13	-10.6 ± 2.6	-16.4 ± 2.7	SPM4	4.2 ± 1.1	16090452-3921125
Sz115	16 09 06.2	-39 08 52	-12.9 ± 3.4	-18.4 ± 3.4	SPM4	4.8 ± 1.3	16090621-3908518
Sz134	16 09 12.3	-41 40 25	-13.3 ± 2.1	-20.4 ± 2.2	SPM4	5.2 ± 1.2	16091226-4140249
RXJ1609.4-3850	16 09 27.4	-38 50 19	-10.3 ± 2.0	-17.3 ± 2.0	SPM4	4.3 ± 1.0	16092739-3850186
Sz116	16 09 42.6	-39 19 41	-16.4 ± 2.1	-26.1 ± 2.2	SPM4	6.6 ± 1.5	16094258-3919407
Sz117	16 09 44.4	-39 13 30	-12.7 ± 2.5	-20.1 ± 2.5	SPM4	5.1 ± 1.2	16094434-3913301
Sz118	16 09 48.6	-39 11 17	-13.3 ± 9.0	-13.4 ± 8.7	SPM4	3.9 ± 2.1	16094864-3911169
RXJ1609.9-3923	16 09 54.0	-39 23 27	-7.6 ± 2.1	-14.9 ± 2.2	SPM4	3.6 ± 0.9	16095399-3923275
Sz119	16 09 57.1	-38 59 48	-11.9 ± 2.3	-24.6 ± 2.4	SPM4	5.8 ± 1.4	16095707-3859479
Sz120	16 10 10.6	-40 07 44	-5.2 ± 1.1	-6.4 ± 1.2	TYCHO2	1.7 ± 0.5	16101054-4007437
Sz122	16 10 16.4	-39 08 05	-15.9 ± 2.4	-21.9 ± 2.4	SPM4	5.7 ± 1.4	16101642-3908050
Sz123	16 10 51.6	-38 53 14	-7.1 ± 2.5	-16.9 ± 2.6	SPM4	3.9 ± 1.0	16105158-3853137
RXJ1612.0-3840	16 12 01.4	-38 40 27	-9.8 ± 1.0	-15.7 ± 1.1	SPM4	3.9 ± 0.9	16120140-3840276
SSTc2dJ161207.6-381324	16 12 07.6	-38 13 24	-6.9 ± 1.3	-13.6 ± 1.3	SPM4	3.2 ± 0.8	16120761-3813242
RXJ1612.3-4012	16 12 22.1	-40 12 52	-22.8 ± 1.6	-42.6 ± 1.7	SPM4	10.3 ± 2.3	16122204-4012522
SSTc2dJ161243.8-381503	16 12 43.7	-38 15 03	-6.8 ± 1.4	-12.4 ± 1.4	SPM4	3.0 ± 0.7	16124373-3815031
RXJ1614.4-3808	16 14 26.4	-38 08 00	-15.2 ± 0.7	-22.2 ± 0.7	SPM4	5.7 ± 1.3	16142637-3807597
HD147402*	16 23 29.6	-39 58 00	-11.6 ± 1.0	-24.2 ± 1.2	SPM4	5.7 ± 1.3	16232955-3958008

Notes. The symbol “*” indicates those stars whose membership status (Lupus or UCL) is doubtful in the literature. For each star we provide the most usual identifier, position (epoch 2000), proper motion, source of proper motion, parallax, and the 2MASS identifier.

Appendix A: Error propagation of parallaxes

The parallax uncertainty for those stars with known RVs is obtained by error propagation of Eq. (4) and it is given by

$$\sigma_\pi^2 = \left(\frac{A}{V_r \tan \lambda} \right)^2 \sigma_{\mu_\parallel}^2 + \left(\frac{A \mu_\parallel}{V_r^2 \tan \lambda} \right)^2 \sigma_{V_r}^2 + \left(\frac{A \mu_\parallel}{V_r \sin^2 \lambda} \right)^2 \sigma_\lambda^2. \quad (\text{A.1})$$

While σ_{μ_\parallel} and σ_{V_r} refer to errors on observational quantities (i.e., proper motions and RVs), the use of σ_λ in eq. (A.1) is not straightforward. Galli et al. (2012) performed extensive simulations that convincingly demonstrate that the precision of the CP position is influenced by several parameters. The increasing velocity dispersion of the cluster and the existence of possible interlopers in the moving group also play an important role when evaluating the precision and accuracy of the CP position. These sources of errors can be roughly divided into two parts: (i) observational errors that arise mainly from proper motion errors (since errors on stellar position can be neglected to a first-order approximation), and (ii) geometric effects (e.g., angular distance from the CP to the moving group, cluster concentration, distance, and number of group members). To correctly introduce the CP errors in the parallax uncertainty, one needs to separate the contribution of these effects, otherwise the error budget due to proper motions will be considered twice in Eq. (A.1). To do so, we set the proper motion errors to zero (i.e., $\sigma_{\mu_{\alpha,\delta}} = 0$). Then, we use Eq. (19) of de Bruijne (1999) to estimate the velocity dispersion of the Lupus moving group that results from the peculiar motion of the stars given by the μ_\perp statistics. This procedure yields $\sigma_{v,\perp} = 0.7_{-0.2}^{+0.4}$ km/s and confirms the adopted value of 1 km/s as the one-dimensional velocity dispersion of the moving group used in our CP analysis (see Sect. 5.1). By adopting $\sigma_v = 0.7$ km/s and $\sigma_{\mu_{\alpha,\delta}} = 0$, the uncertainties on the CP position decrease to $(\sigma_{\alpha_{cp}}, \sigma_{\delta_{cp}}) = (1.6^\circ, 1.2^\circ)$ yielding $\sigma_\lambda \simeq 2.0^\circ$. This result represents a more realistic estimate of the CP error budget due to geometric effects, not including proper motions errors, to be used in the error propagation of parallaxes.

Appendix B: Notes on radial velocities

One important point is that the observed RVs for Lupus stars are expected to be lower than to other SFRs, such as Taurus-Auriga and Chamaeleon (see Bertout & Genova 2006; James et al. 2006). The average value and standard deviation of the RVs presented in Table 4 for Lupus stars is $\bar{V}_r = 2.7 \pm 1.9$ km/s, and the average error is $\sigma_{V_r} = 0.5$ km/s. Here we investigate the errors on parallaxes and space velocities caused by uncertainties in RVs. A small variation ΔV_r in RVs accounts for the variation $\Delta\pi$ in parallaxes that can be approximated by

$$\Delta\pi \simeq \frac{A \mu_\parallel}{\tan \lambda} \left(\frac{\Delta V_r}{V_r^2} \right). \quad (\text{B.1})$$

This shifts the space velocity of the star by ΔV_{space} that is given as

$$\Delta V_{space} \simeq \frac{A \mu_\parallel}{\sin \lambda} \left(\frac{\Delta\pi}{\pi^2} \right). \quad (\text{B.2})$$

Using the values of position, proper motion, and radial velocities given in Table 2 for the on-cloud population, and the CP solution derived in Sect. 5.3, we note that a small shift $\Delta V_r = 0.5$ km/s in the measured RVs accounts for $\Delta\pi \simeq 1.4$ mas, and consequently, $\Delta V_{space} \simeq 4$ km/s. We thus emphasize that high-precision RVs are needed to derive reliable kinematic parallaxes of Lupus stars.